

Echo-Planar Magnetic Resonance Imaging of Human Brain Activation

P. A. Bandettini and E. C. Wong

Introduction

Development of new methods to image the thinking human brain is fundamental to unraveling the principles of its workings. The latest and most promising functional brain activation imaging techniques to emerge have been those which use magnetic resonance imaging (MRI). The array of MRI-based techniques used for the study of brain activation has been termed functional MRI (fMRI). Echo-planar imaging (EPI), an ultrafast MRI technique [1-5], has been and continues to be ubiquitous in the ongoing development and application of fMRI in general. In the growing number of centers that have EPI capability, it is the fMRI method of choice. An overview of EPI in the study of human brain function is given in this chapter. A brief overview of fMRI is first given. Second, details regarding the implementation of EPI for fMRI, as of May, 1995, are described. Lastly, EPI is discussed in the context of four developing areas in fMRI: imaging platform or methodology development, contrast mechanism research, postprocessing development, and applications. In the areas of imaging platform development and contrast mechanism research, several examples demonstrating the utility of EPI are given.

fMRI Overview

Brain Activation

When a population of neurons experiences membrane polarity changes during activation, measurable electrical and magnetic changes in the brain are created [6-12]. Because of the energy requirements of membrane repolarization and neurotransmitter synthesis, brain activation also causes a measurable increase in neuronal metabolism [6-8, 13-18]. Through incompletely understood mechanisms [6, 19-30] these changes are accompanied by changes in blood flow [6-8, 19-36], volume [37-40], and oxygenation [39-43]. All techniques for assessing human brain function are based on the detection and measurement of these electrical, magnetic, metabolic, and hemodynamic changes that are spatially and temporally associated with neuronal activation.

MRI of Cerebrovascular Physiology

Pioneering work has shown that MRI can be used to map several types of cerebrovascular information. With MRI, one can create (a) maps of cerebral blood volume [38, 44–50] and flow [3, 51–53] and (b) maps of changes in cerebral blood volume [38], flow [3, 53, 54], and oxygenation [54–65].

Blood Volume

A technique developed by Belliveau and Rosen et al. [44–46] utilizes the susceptibility contrast produced by intravascular paramagnetic contrast agents and the high-speed imaging capabilities of EPI to create maps of human cerebral blood volume. A bolus of paramagnetic contrast agent is injected and T2- or T2*-weighted images are obtained at the rate of about one image per second. As the contrast agent passes through the microvasculature, susceptibility gradients (magnetic field distortions) are produced. These gradients cause an intravoxel dephasing of extravascular proton spins, resulting in a transient signal attenuation. The signal attenuation is linearly proportional to the concentration of contrast agent [44, 45, 66], which in turn is a function of blood volume.

Changes in blood volume that occur during hemodynamic stresses or during brain activation may then be created by subtraction of two maps: one during a "resting" state and one during the hemodynamic stress or during activation [38]. The use of this method marked the first time that hemodynamic changes accompanying human brain activation were mapped with MRI.

Blood Flow

Blood flow spans several size and velocity scales. Imaging of large cerebral vessels having rapid flow rates by MR cerebral angiography [50, 67, 68] has been a clinical technique since the middle 1980s.

Imaging and quantification of microvascular flow in the brain has been not yet been fully realized. Two techniques for MRI of cerebral microvasculature have been proposed. LeBihan et al. proposed a technique in which capillary flow is modeled as a fast diffusive process [69–72]. With this intravoxel incoherent motion (IVIM) model, it has been suggested that techniques used to measure diffusion can be used to measure microvascular flow. This technique, while theoretically feasible, has practical limitations which include contamination from cerebral spinal fluid and other tissue motion on the same velocity scales [73] and the requirement of a signal-to-noise ratio (SNR) that is not practically achieved in most imaging studies [74].

A second technique for quantifying microvascular blood flow entails MR detection of inflowing labeled arterial water spins, and was first demonstrated in animals [51, 52]. With this technique blood water flowing to the brain is radiofrequency (RF) saturated outside the imaging plane (usually in the neck region). Because of the relatively long blood T1 times, saturated spins are able

to maintain much of their magnetization state as they travel into the plane of interest and exchange, at the capillary level, longitudinal magnetization with bulk water in the brain. The resulting regional concentration of labeled spins in tissue is a function of regional tissue blood flow.

A recently developed extension of this flow imaging technique, named echo-planar imaging with signal targeting and alternating RF (EPSTAR), has been used to map both macrovascular and microvascular flow [3, 75] in humans. This technique is based on the idea of subtracting two image data sets that are identical except for differences in longitudinal magnetization arising from inflowing spins. One data set is acquired after a remote 180° pulse is applied to invert the inflowing arterial spins. The first set is subtracted from a second data set, acquired without the inversion pulse, thus giving a difference map which is a function of flow.

This technique can be made sensitive to different levels of flow velocity by varying the delay time between the inversion pulse and the image acquisition. Maps of arterial flow are created using a relatively short inversion pulse-acquisition delay time of 400 ms. Maps of microvascular flow and exchange processes are created using an inversion pulse-acquisition delay time of 1000 ms or more. After the 1000-ms waiting period tagged magnetization is either within the capillary bed or in the extravascular space in the immediate vicinity of capillaries.

With the use of flow map subtraction changes in blood flow corresponding to hemodynamic stress or brain activation can be mapped as well. The two maps can then be subtracted to reveal regions where changes in flow have occurred [3, 75].

An alternative flow sensitive method is performed by application of the inversion pulse in the same plane. In this case the image intensity is weighted not only by modulation of longitudinal magnetization by flowing spins but also by other MR parameters that normally contribute to image intensity and contrast (proton density, T1, T2). Therefore the application of an inversion pulse in the same plane only allows for observation of changes in flow that occur with hemodynamic stress or brain activation. This technique was first implemented by Kwong et al. [54] to observe activation-induced flow changes in the human brain. In this seminal study activation-induced signal changes associated with local changes in blood oxygenation were also observed.

Blood Oxygenation

In 1932 Pauling et al. [76] discovered that the magnetic susceptibility of hemoglobin is sensitive to its oxygen saturation. The susceptibility of red blood cells decreases linearly from a fully oxygenated value of $-0.26 \pm 0.07 \times 10^{-6}$ (CGS units) to a fully deoxygenated value of $0.157 \pm 0.07 \times 10^{-6}$, giving a difference in susceptibility of 0.18×10^{-6} between 100% blood oxygenation and 0% blood oxygenation states [77]. This susceptibility difference results from the fact that oxyhemoglobin contains diamagnetic oxygen-bound iron and deoxyhemoglobin contains paramagnetic iron [76, 78, 79].

In 1982 Thulborn et al. [79] demonstrated that the transverse relaxation rate, R_2 (or $1/T_2$), of blood decreases with an increase in blood oxygenation. Because minimal changes in T_1 of whole blood were observed upon the oxygenation changes, it was suggested that the primary mechanism of relaxation change is related to diffusion of spins through susceptibility-induced gradients (which affects T_2 relaxation) and not due to dipolar interactions (which affects T_1 and T_2 relaxation). The R_2 dependence of blood on its oxygen saturation has been confirmed by several other studies [77, 80–90].

In 1990 pioneering work of Ogawa et al. [59–61] and Turner et al. [63] demonstrated that MR signal in the vicinity of vessels and in perfused brain tissue decreases with a decrease in blood oxygenation. This type of physiological contrast was coined blood oxygenation level dependent (BOLD) contrast by Ogawa et al. [61].

The use of BOLD contrast for the observation of brain activation was first demonstrated in August of 1991 at the 10th Annual Meeting of the Society of Magnetic Resonance in Medicine [91]. The first papers demonstrating the technique, published in July 1992, reported human brain activation in the primary visual cortex [54, 62] and motor cortex [54, 56]. Two [54, 56] of the first three reports of this technique involved the use of EPI. In these experiments a small but significant local signal increase in activated cortical regions was observed using susceptibility-weighted, gradient-echo pulse sequences.

The working model constructed to explain these observations was that an increase in neuronal activity causes local vasodilatation which, in turn, causes an increase in blood flow. This results in an excess of oxygenated hemoglobin beyond the metabolic need, thus *reducing* the proportion of paramagnetic deoxyhemoglobin in the vasculature. This hemodynamic phenomenon had previously been suggested using other techniques [40–42], and later came to the attention of MR investigators attempting to explain these localized activation-induced MR signal increases. A reduction in deoxyhemoglobin in the vasculature causes a reduction in susceptibility differences in the vicinity of venules, veins, and red blood cells within veins, thereby causing an increase in spin coherence (increase in T_2 and T_2^*) and therefore an increase in signal in T_2^* - and/or T_2 -weighted sequences.

Presently the most widely used fMRI technique for the noninvasive mapping of human brain activity is high-speed gradient-echo imaging using BOLD contrast. The reasons for this are that (a) gradient-echo T_2^* -sensitive techniques have demonstrated higher activation-induced signal change contrast than techniques having T_2 -weighted, flow-sensitive, and blood volume-sensitive techniques, and (b) BOLD contrast can be obtained using more widely available high-speed multi-shot non-EPI techniques.

Several ongoing issues regarding interpretation, postprocessing, and the limits of applicability of fMRI remain. As is shown below, EPI is a technique that because of its speed, efficiency, and robustness lends itself well to the understanding and resolution of these issues.

Implementation of EPI for fMRI

Several issues regarding the implementation of EPI are briefly addressed here in the context of fMRI. These include issues of spatial resolution, hardware, biological limitations, artifacts, software, and data handling.

Spatial resolution in single-shot EPI is limited either by the area of k space that can be critically sampled in approximately one $T2^*$ period or by the system bandwidth [92]. The area of k space that can be covered can be limited by the velocity in k space (gradient amplitude) or the acceleration in k space (gradient slew rate) and is typically limited by both. The tradeoff between gradient amplitude and gradient slew rate in the design of the gradient system is one that has application-specific optima; systems that are designed specifically for single-shot EPI therefore generally perform this function most efficiently.

The requirement for strong and rapidly switching gradients can be satisfied by increasing the gradient amplifier power, implementing resonant gradient technology, or by reducing the inductance of the gradient coils such that they can be driven by conventional gradient amplifiers. The latter strategy may be implemented by using a gradient coil that is localized only to the head. Figure 1 illustrates an example of a local gradient coil used for EPI on an otherwise conventional system. The three-axis balanced torque gradient coil (ID = 30 cm, length = 37 cm) was designed and constructed by Wong [93]. The method of design was gradient descent [94]. The gradient fields were optimized for a region that covers the human brain (cylinder of diameter 18.75 cm and length 16.5 cm.) The maximum gradient strengths (G/cm 100 A) are 2.272 G/cm for X, 2.336 G/cm for Y, and 2.487 G/cm for Z. As a result of the low coil inductance (0.149 mH for X, 0.174 mH for Y, and 0.076 mH for Z), the minimum rise time from zero amplitude to full scale is approximately 50 μ s. For a comprehensive review on techniques for designing gradient coils, please refer to Turner [95]. While the use of local gradient coils makes single-shot EPI possible on standard clinical systems, the system bandwidth may limit its implementation. Inadequate bandwidths may limit the useful gradient amplitude, thereby reducing spatial resolution. Lastly, single-shot EPI can be carried out on a conventional imaging system

Fig. 1. The three-axis balanced torque head gradient coil used for EPI on conventional clinical MRI scanners. ID = 30 cm; length = 37 cm. The maximum gradient strengths (G/cm at 100 A) are 2.272 G/cm for X, 2.336 G/cm for Y, and 2.487 G/cm for Z. Inductances are 0.149 mH for X, 0.174 mH for Y, and 0.076 mH for Z. Minimum rise time from zero amplitude to full scale is approximately 50 μ s



without the use of local gradient coils by simply using a large field of view and/or a small image matrix size [96].

A major non-hardware-related limitation on gradient slew rate is the biological threshold for neuronal stimulation due to time-varying magnetic fields. At present high-performance gradient systems (either local gradient coils or high-powered whole body systems) are capable of exceeding the guidelines of the United States Food and Drug Administration on field slew rate (dB/dt), and the optimization of EPI pulse sequences is strongly affected by dB/dt considerations. Taking all these considerations into account, optimal spatial resolution in the human head for single-shot EPI is achieved at these approximate values: matrix of 128×128 , bandwidth of 250 kHz, gradient strength of 4 G/cm, and data acquisition window of 80 ms.

The requirements for successful implementation of EPI for fMRI are not limited to hardware. In most cases phase correction algorithms are a necessity to compensate for timing errors related to imperfections in the gradients, gradient-induced eddy currents, and static field inhomogeneities. The timing errors generally manifest themselves as Nyquist ghosts. Even if the ghosts are not completely eliminated from each image, they usually remain stable in intensity and location from image to image over time. Also, since the location of the ghosts is usually outside of the head, they usually do not cause significant problems in the interpretation of the functional images.

Because of the long-sampling time and artifactual phase modulation, two other types of off-resonance related artifacts exist in EPI: signal dropout, and image distortion.

Signal dropout is primarily due to intravoxel phase dispersion resulting from through plane variation of magnetic field. This effect is common to all gradient-recalled imaging techniques, and is dependent primarily on the TE and slice thickness and the local shim in specific regions of the brain. The problem of signal dropout in gradient-echo sequences can be reduced by reduction of the voxel volume. Therefore gradient-echo image quality, if acquired at the base of the brain where large susceptibility gradients exist, is improved by reduction of voxel volume. Also, this effect is greatly reduced in spin-echo EPI as well as other spin-echo techniques because the macroscopic off-resonance effects are refocused at the echo time.

Image distortion is caused by the phase modulation that occurs during data acquisition. Because the artifactual phase modulation is linear in time, it is directly proportional to the data acquisition time. In EPI this linear phase modulation creates primarily a linear distortion of the image in the phase encode direction whose magnitude is given by the Fourier shift theorem. If the phase modulation is 2π across the data acquisition window, the shift in image space is one pixel. Thus for a 40-ms data acquisition window a signal that is 25 Hz off resonance is shifted by one pixel. Several postprocessing methods have been put forward for correcting image distortion in EPI [97-99].

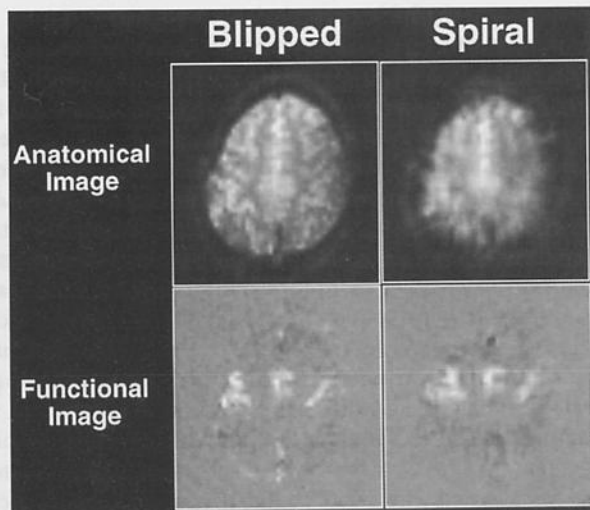
The image distortion effect is present in conventional imaging techniques as well. For example, if a conventional spin-warp technique is used with the same resolution and the same data acquisition time as used with EPI, the distortion is the same. However, the distortion in spin-warp imaging techniques is typically

smaller because the data acquisition times are shorter and the resolution is higher, both of which decrease the magnitude of the distortion. It should be noted, however, that it is exactly these two parameters, higher resolution and shorter data acquisition times, that decreases the SNR per unit time of spin-warp techniques relative to EPI.

The artifacts caused by macroscopic off-resonance effects are also dependent on k space traversal path. In the case of spiral imaging off-resonance effects are not manifested as Nyquist ghosts or image distortion but as blurring [4, 100]. Figure 2 shows a comparison of single-shot blipped EPI (40 ms acquisition window) and single-shot spiral EPI (28 ms acquisition window). The anatomical images differ in that the blipped image is sharper but more distorted. The spiral image shows apparently less distortion but much more blurring in the radial direction. A time course of blipped and spiral images were collected during which the subject performed periodic bilateral finger tapping. Functional correlation images, shown below the anatomical images, were created by calculation of the vector product of a reference waveform with the time course of each voxel [101]. Note that both sequences reveal signal enhancement in the supplementary and primary motor cortex and possibly the somatosensory cortex. The locations and extents of the activated regions appear different due to the different sensitivity to gross off-resonance effects. It should also be noted that because the central part of k space is usually covered very early in the spiral path, the sequence is less sensitive to flow than blipped sequences are [100, 102].

Another practical but significant factor to be considered when performing fMRI with EPI is the rapidity with which large amounts of data are collected. This data may then go through several additional transformations (adding to the total required data storage capacity) before a functional image is created. If ten slices having 64×64 resolution are acquired every 2 s (typical for multislice fMRI), the data acquisition rate is approximately 2 MB per minute.

Fig. 2. Demonstration of the relative sensitivity of single-shot blipped and spiral EPI to off-resonance effects. *Left*, single-shot blipped EPI is sharper but distorted; *right*, single-shot circular spiral EPI is not distorted but is more blurred. Functional correlation images demonstrate similar functional contrast but slightly different locations



Research in fMRI

Research in fMRI can be divided into four overlapping and interdependent categories: functional imaging hardware and pulse sequence development, contrast mechanism research, postprocessing development, and applications. In all of these categories the use of EPI has been extensive, primarily because for most applications its robustness outweighs its limitations. In the remainder of the chapter the role of EPI in each of these research categories is discussed.

fMRI Hardware and Pulse Sequence Development

The first fMRI experiments were carried out using EPI at 1.0 [103], 1.5 [54, 56, 64, 91, 104, 105], 2.1 [57], 3.0 [106], and 4 T [64], and fast multi-shot gradient-recalled imaging techniques at 1.5 [64], 2 [58, 107], and 4 T [62]. Platforms for fMRI vary considerably in terms of pulse sequence, field strength, gradient hardware, and RF coil hardware. Generally, fMRI platform evolution has been in the direction of increased functional contrast-to-noise ratio (CNR), temporal resolution, spatial resolution, and hemodynamic specificity.

Functional Contrast-to-Noise Ratio

Functional contrast relates to the detection of activation-induced signal changes in space (as opposed to nonactivated regions) and time (as opposed resting state signal). The most fundamental of needs in fMRI is a high functional CNR to detect small signal changes. When using gradient-echo sequences, maximal susceptibility contrast is achieved by using TE approximately equal to $T2^*$ [57, 108, 109]. In addition, studies have shown, largely in agreement with predictions of several susceptibility contrast models [66, 110–114], that BOLD contrast increases with field strength [62, 64, 106, 108, 115, 116]. However, because of its sensitivity to off-resonance effects, performance of EPI is more difficult, but still possible, at higher field strengths [64, 106, 116–118].

An alternative to increasing contrast is reduction in the noise relative to the image signal intensity. Several simple strategies are commonly used in fMRI to increase SNR – most of which EPI is well suited for. The use of a relatively long TR, 90° flip angle, and temporal averaging of several hundred images can be performed in an experimentally feasible amount of time using EPI. Also, with EPI the long data acquisition times that are typically used in order to achieve acceptable spatial resolution are approximately equal to the $T2^*$ of gray matter – optimal from the point of view of maximizing the SNR.

Many of the sources of signal contamination are not from system or thermal noise but rather from cardiac and respiration-related pulsatile motion [100, 102, 119–123] or subject movement [124] or possibly from susceptibility gradient variations related to spontaneous changes in flow [125, 126] or respiration-related changes in chest cavity size, which has been suggested to cause changes in B_0 , as far away as the head region (Ugurbil, personal communication). Therefore

the CNR can also be increased by reduction of signal fluctuations that contribute to the noise.

In conventional multi-shot techniques pulsatile motion during data acquisition has been shown to cause variation in k space registration which primarily causes nonrepeatable ghosting variations across each image, adding significantly to the noise [100, 102]. With EPI physiological motion is "frozen" by the short 40-ms acquisition time of all k space, enabling stable line-to-line registration across each image during acquisition – thus reducing this source of noise significantly.

In EPI gross displacement generally manifests itself as misregistration at edges and as some isolated signal propagation in the phase encode direction from rapidly flowing or moving spins [127]. Asymmetric spin-echo EPI, with similar contrast weighting as gradient-echo EPI, has demonstrated a reduction in artifacts caused by rapidly flowing and pulsatile spins because the 180° pulse does not refocus rapidly flowing spins [128].

Among non-EPI techniques multi-shot spiral-scan sequences [100, 102], sequences employing oblique motion compensation [129], and sequences employing navigator pulses [130] have all demonstrated more signal stability over time and less artifactual signal changes than standard two- or three-dimensional Fourier transform multi-shot techniques.

The SNR can also be increased by the use of region-selective RF coils. Optimally, the RF coil should couple only to the regions that are being studied, such as surface coils over the occipital pole in visual stimulation studies. However, it is becoming increasingly desirable for most functional imaging studies to observe the entire brain. For whole-brain studies whole-head quadrature coils commonly used clinically for head and neck imaging are suboptimal because they couple to other tissue that is not of interest, causing an unnecessary increase in noise. Recently quadrature whole-brain transmit-receive coils that couple predominantly to the brain have been implemented for fMRI [131, 132].

Temporal Resolution

Because the fMRI signal change is based on hemodynamic changes, the practical upper limit on functional temporal resolution is determined by MRI SNR and by the variation of the hemodynamic response latency in space and in time [133–139]. These variations may be due to differences in neuronal activation characteristics across tasks [137, 138], to differences in vessel size [133, 134], or to other physiological or anatomical differences. In primary visual and motor cortex the latency of the hemodynamic response is approximately 5–8 s from stimulus onset to 90% maximum, and 5–9 s from stimulus cessation to 10% above baseline [54, 57, 101, 138–141]. This latency has been described as a shifting and smoothing transformation of the neuronal input [142]. Given the variations of the hemodynamic response, the upper limit of temporal resolution discrimination has been empirically determined to be on the order of 1 s [136] or less [143]. With greater specificity for hemodynamic scale, higher SNR, and innovative experimental design this upper limit on temporal resolution may be increased even further.

For many types of investigations it may be desirable to use experimental paradigms similar to those used in event-related potential recordings or magnetoencephalography [144], in which multiple runs of transient stimuli are averaged together. For this type of paradigm, requiring rapid sampling and high SNR for a very brief duration, EPI is optimal. As a side note, because of the brief collection time of EPI relative to typical TR values the between-image waiting time allows performance of EEG in the scanner during the imaging session [145].

The type of neuronal and/or hemodynamic information that may be obtained from signals elicited from brief stimuli paradigms may be different from the information elicited by longer duration activation times. Transient activation durations (<1 s) are detectable as MR signal changes which begin to increase 2 s after the activation onset and plateau at 3–4 s after activation [135, 139, 140, 143, 146]. Figure 3 shows signal intensity vs. time from a region in motor cortex in which the subject performed a finger tapping task for 0.5 s.

Unique information may also be obtained from rapidly sampled and highly averaged time course data. As an example of unique hemodynamic information obtained in this manner, a small decrease in signal before the subsequent signal increase with photic stimulation has been observed by Menon et al. [117, 118] using EPI at 4 T.

The study of the underlying noise from which activation-induced signal changes must be separated is also highly important for both detailed physiological studies and postprocessing development. Frequency components contained in signal fluctuations have been characterized using EPI [120, 121, 147]. An example is given of how the use of EPI allows for characterization of signal fluctuations. In this study the a time course of images were rapidly collected during rest. After reaching steady state magnetization 125 images were collected in 25 s (voxel volume = $3.75 \times 3.75 \times 10$ mm³, flip angle = 60° , TR = 200 ms). Signal intensity was measured from a voxel in the sagittal sinus. Figure 4 shows a plot of signal vs. time from a region containing the sagittal sinus and the Fourier transform of that signal. The peak at about 45 beats per minute corresponds to the volunteer's heart rate (a marathon runner). An anatomical image of the axial slice observed

Fig. 3. Signal intensity (from a single run) vs. time from a region in motor cortex. TR/TE = 1000 ms/40 ms. Two 0.5-s episodes of finger movement were performed. Signal intensity begins to increase 2 s after activation, peaks 4–5 s after activation, then returns to baseline 8–9 s after activation

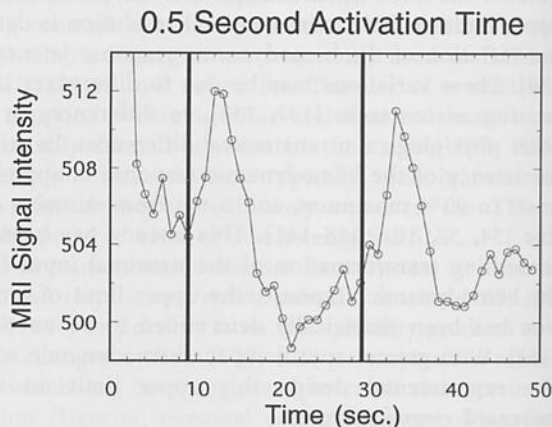
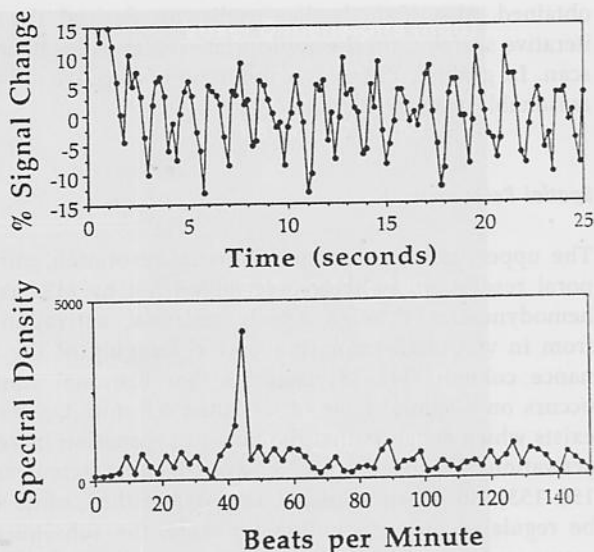


Fig. 4. Signal intensity vs. time from a voxel in the sagittal sinus. TE/TR = 40 ms/200 ms. Below, Fourier transform of the signal vs. time plot, revealing a peak at the heart-rate

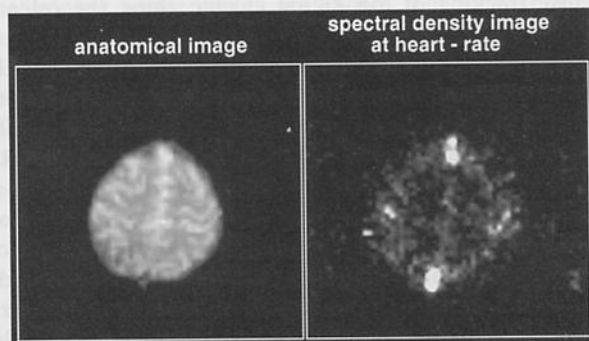


and the spectral density image at that frequency is shown in Fig. 5. High signal intensity regions in this spectral density image correspond to voxels containing cerebral spinal fluid and large vessels. The source of these signal changes is likely periodic time-of-flight inflow effects of unsaturated magnetization.

With the use of EPI approximately ten images may be obtained per second – giving the option to image the entire brain in under 2 s or to sample a smaller number of imaging planes to allow a more dense sampling of the time course. Another possibility in EPI is to sample less densely in space but to cover a large volume in a single shot. This technique is known as echo-volume imaging [1, 5, 148].

The more rapid the feedback of fMRI data, the more easily experiments can be fine-tuned or appropriately adjusted. If EPI is used in conjunction with real-time functional image formation [149], the quality of functional images can be monitored during time course scanning until the desired functional image quality is

Fig. 5. Anatomical image and spectral density image at the above heart rate frequency peak, revealing regions of periodic signal changes in the brain



obtained. Also, if single slice studies are desired, the use of EPI can allow for an iterative search until the appropriate region is located – similar to a clinical scout scan. In general, EPI allows this type of iterative approach to be performed in a reasonable amount of time.

Spatial Resolution

The upper limit on functional spatial resolution, similarly to the limit of temporal resolution, is likely determined not by MRI resolution limits but by the hemodynamics through which neuronal activation is transduced. Evidence from *in vivo* high-resolution optical imaging of the activation of ocular dominance columns [41–43] suggests that neuronal control of blood oxygenation occurs on a spatial scale of less than 0.5 mm. On the other hand, MR evidence exists which suggests that the blood oxygenation increases that occur upon brain activation may be more extensive than the actual activated regions [133, 134, 150–153]. In other words, it is possible that, while the local oxygenation may be regulated on a submillimeter scale, the subsequent changes in oxygenation may occur on a larger scale due to a “spill-over” effect.

To achieve the goal of high spatial resolution fMRI a high functional CNR and reduced signal contribution from draining veins is necessary. Greater hemodynamic specificity, accomplished by proper pulse sequence choice, innovative activation protocol design, or proper interpretation of signal change latency, may allow greater functional spatial resolution. If the contribution to activation-induced signal changes from larger collecting veins or arteries can be easily identified and/or eliminated, not only is confidence in the brain activation localization increased, but also the upper limits of spatial resolution are determined by scanner resolution and BOLD CNR rather than variations in vessel architecture.

Currently voxel volumes as low as 1.2 μl have been obtained by functional fast low-angle shot techniques at 4 T [115], and experiments specifically devoted to probing the upper limits of functional spatial resolution, using spiral scan techniques, have shown that fMRI can reveal activity localized to patches of cortex having a size of about 1.35 mm [154]. These studies and others carried out using EPI [155] and multi-shot spiral scanning [154, 156] have observed a close tracking of MR signal change along the calcarine fissure as the location of visual stimuli was varied.

The voxel dimensions typically used in single-shot EPI studies are in the range of 3–4 mm, in plane, and have 4- to 10-mm slice thicknesses. As mentioned, these dimensions are determined by practical limitations such as readout window length, sampling bandwidth, limits of dB/dt, SNR, and data storage capacity. In spite of these limitations higher resolution single-shot EPI can be performed in some situations. Figure 6 presents an example of four functional studies using progressively higher resolution single-shot gradient-echo EPI. The imaging plane contains the motor cortex. The subject was instructed to perform periodic bilateral finger tapping. Anatomical and functional correlation images and corresponding voxel dimensions are shown. The size of the activated region appears

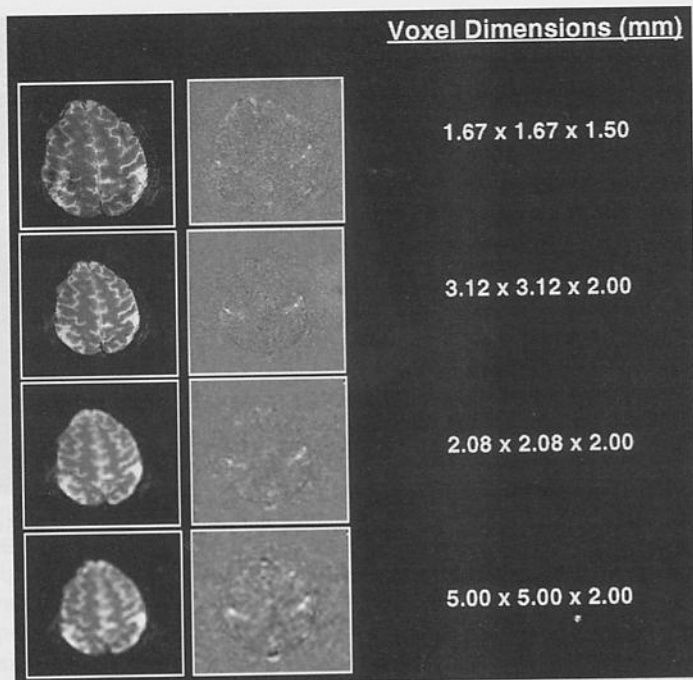


Fig. 6. Demonstration of progressively higher resolution single-shot gradient-echo EPI. Anatomical and functional correlation images from a single subject performing bilateral finger movement

to decrease as the spatial resolution is increased. At low resolution either more subtle capillary-related signal changes are being observed (due to the higher SNR) along with large vessel effects, or large vessel effects are simply being partially volumed with inactive areas in the same large voxels.

Other ways to bypass the practical scanner limits in spatial resolution include partial k space acquisition [4] and multi-shot mosaic or interleaved EPI [4, 157, 158]. An example of multi-shot interleaved EPI in the context of fMRI is given in Fig. 7 (images provided by S. Tan). Axial anatomical and corresponding functional correlation images containing motor cortex are shown. The subject performed cyclic bilateral finger tapping. The highest resolution image was obtained in 4 s. The voxel dimensions for this image are $0.937 \times 0.937 \times 5$ mm. The activated regions, while reduced in size, are clearly visible. In many fMRI situations multi-shot EPI may be the optimum compromise between spatial resolution, SNR, and temporal resolution for fMRI.

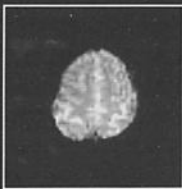
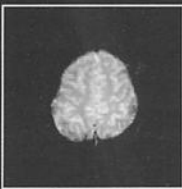
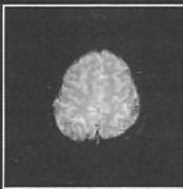
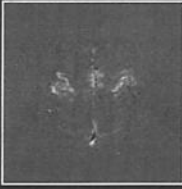
Excitations	1	2	4	8
Matrix Size	64x64	128x128	256x128	256x256
Anatomical Image				
Functional Image				

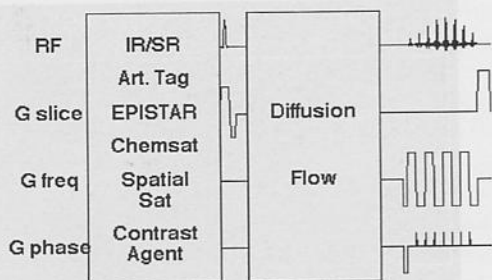
Fig. 7. Demonstration of progressively higher resolution multi-shot interleaved EPI. Anatomical and functional correlation images from a single subject performing bilateral finger movement. (Images were provided by S. Tan)

Hemodynamic Specificity

The interpretability of fMRI depends to a large degree on the specific hemodynamic sensitization that is possible. Changes in flow, volume, and oxygenation can be selectively observed with fMRI: volume changes – using rapidly obtained T2*- or T2-weighted sequences in combination with bolus administration of a paramagnetic contrast agent [38], flow changes – using inversion recovery [53, 54] or short TR/short TE sequences [151, 159], and oxygenation changes – using T2*- or T2-weighted sequences [54, 56–65, 109]. Also, intravascular vs. extravascular effects may be discerned by appropriate choice of velocity-dephasing gradients [160–163]. Large vessel vs. small vessel effects may be selectively observed by careful interpretation of relative activation -induced R2 and R2* changes [109, 113, 164, 165] as well as by inspection of high resolution T2*-weighted images at high field strength [108]. Veins in the latter case show up as dark spots in the high resolution T2*-weighted images. Because the typical implementation of single-shot EPI involves the acquisition of one image every RF excitation followed by a waiting period of about 1 s, many of the above-mentioned hemodynamic-specific pulse-sequence manipulations can be applied without any sacrifice in imaging time and without additional contamination from motion artifacts which is especially important in the case of diffusion weighting. Figure 8 illustrates schematically, the types of manipulations that can be easily implemented for hemodynamic specificity using EPI.

A comparison of activation-induced signal change locations across several pulse sequence weightings, keeping all else constant, is given below. Each time course series consisted of 240 sequential images. (TR = 2 s, voxel

Fig. 8. Schematic illustration of the types of contrast manipulations that can be implemented for achieving hemodynamic specificity with EPI



volume = $3.75 \times 3.75 \times 5$ mm.) Total time course length was 480 s. Table 1 displays the EPI pulse sequence parameters used and their respective contrast weightings, based on what has been hypothesized in the literature [3, 51, 52, 54, 113]. During each time course series, sequential, bilateral finger tapping was performed in alternating 20-s rest and 20-s activation cycles. Functional correlation images were then created. Figure 9 displays the first image in each of the six time course series. Figure 10 displays the corresponding functional correlation images showing activation in primary motor cortex regions. In spite of the different hemodynamic specificity of each sequence, the activated regions are similar in location, extent, and shape. However, on closer inspection of a magnification of the images, shown in Fig. 11, a systematic shift in activation foci is apparent. In the $T2^*$ -weighted images the focal points of activation appear more lateral on

Table 1. Pulse sequences and the corresponding image contrast and functional contrast weightings

Sequence	Parameters	Contrast weighting	Flow	Oxygenation	
				BOLD (>20 μ m)	BOLD (<20 μ m)
Inversion recovery	TI = 1200 TR = 2000 TE = 60	High T1 Slight T2	y		x
Asymmetric spin-echo inversion recovery	TI = 1200 TR = 2000 TE = 60 $\tau = 40$	High T1 High T2* Slight T2	y	y	x
Asymmetric spin-echo	TR = 2000 TE = 60 $\tau = 40$	High T2* Slight T2		y	x
Spin-echo	TR = 2000 TE = 60, 100	Slight T2 High T2			x,y
Gradient-echo	TR = 2000 TE = 40	High T2*		y	y

y = high sensitivity, x = low sensitivity, according to the current models, to flow or to changes in blood oxygenation in large (greater than 20 μ m) compartments and small (less than 20 μ m) compartments.

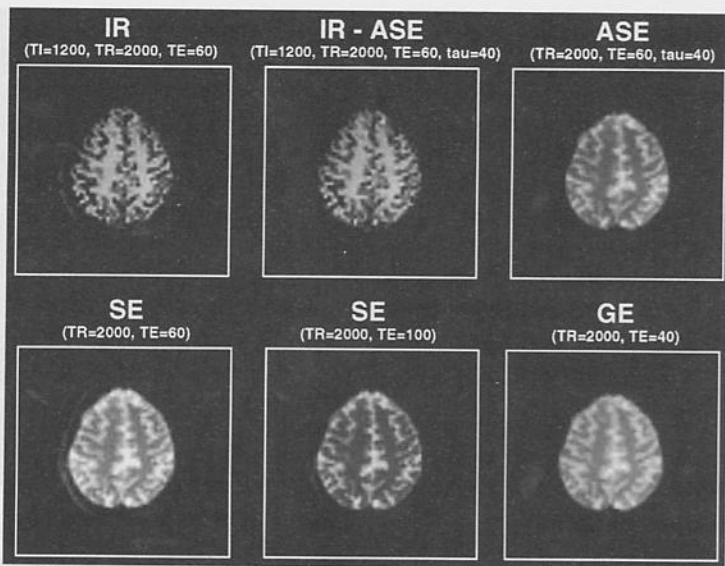


Fig. 9. First image in each of the EPI time course series having different contrast weightings. *IR*, inversion recovery; *ASE*, asymmetric spin echo; *SE*, spin echo; *GE*, gradient echo

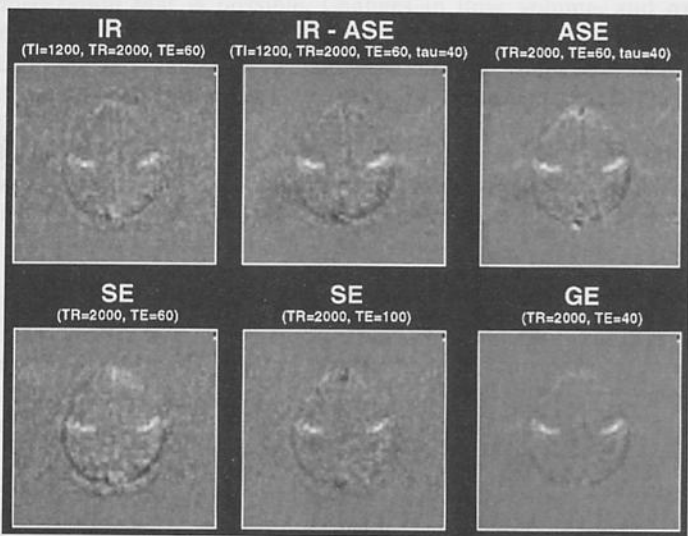


Fig. 10. Functional correlation images created from time course series of corresponding images (Fig. 9). Differences can be seen in functional contrast to noise and artifactual contamination. Overall similarity of activated region locations and extents is apparent. For abbreviations, see Table 1

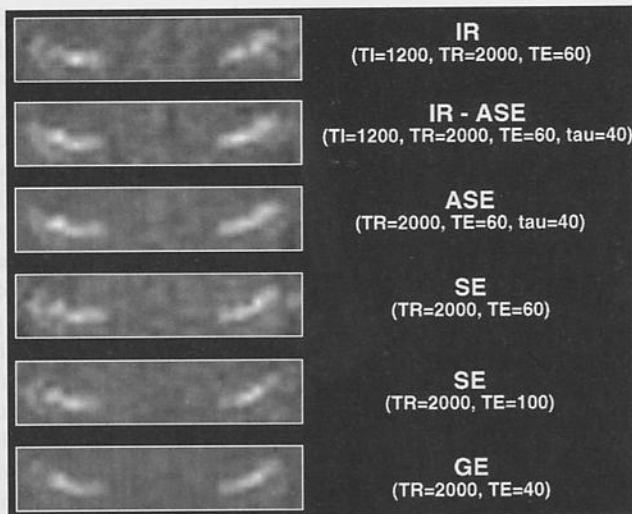


Fig. 11. Magnification of functional correlation images given in Fig. 10. Comparison of the different pulse sequences demonstrates subtle and systematic shifts in activation locations. For abbreviations, see Fig. 9

both sides. In the T1- and the T2-weighted images the focal points are located several millimeters more centrally. In the correlation image that was obtained using the asymmetric spin-echo inversion-recovery sequence, which is both T2*- and T1-weighted, two foci appear on the left side of the image that correspond to the individual foci obtained separately using the other sequences.

While not giving any definitive conclusion about underlying hemodynamic processes, these studies illustrate the flexibility that EPI offers in the time-efficient collection of images having several different contrast weightings. Regardless of the hemodynamic weighting of the pulse sequence it is heartening to note that the regions showing activation in this study predominantly overlap.

Contrast Mechanism Research

Research performed to characterize the details of the fMRI contrast mechanisms has been motivated by the desire to determine a correlation of the magnitude, spatial extent, and timing of the observed MR signal changes with underlying neuronal activation magnitude, extent, and timing. While it is generally accepted that MR signal changes are transduced through neuronally induced hemodynamic changes, the following two relationships are not clear: (a) the relationship between the magnitude, timing, and spatial extent of neuronal activation and the magnitude, timing, and spatial extent of the hemodynamic changes, and (b) the relationship between the degree, timing, and spatial extent of induced hemodynamic changes and the degree, timing, and spatial extent of the MR signal changes.

The difficulty in activation-induced signal change contrast mechanism research is that the *actual* location, magnitude, and timing of neuronal activation is imprecisely known. In general, contrast mechanism studies have involved well-controlled modulation of many potentially significant parameters. By parameter modulation and subsequent comparison with an ever-growing model which includes MR physics, cerebral physiology, and neurology a large amount of convergent information about the relative contributions to MR signal changes has been and continues to be obtained.

Strategies for a more complete understanding of fMRI contrast mechanisms have involved: (a) observation of the dependence of the magnitude, timing, and spatial extent of activation-induced signal changes upon MR parameters such as TE [62, 108, 109, 116, 164–167], TI [3], flip angle [151], B_0 [62, 64, 106, 108, 116], slice thickness and resolution [107, 152, 153, 166], outer volume saturation [159], and diffusion weighting [160–163], (b) observation of the resting signal, and activation-induced signal changes, during different degrees of hemodynamic stress [59–61, 63, 168–173] or during different degrees of neuronal activity (visual flicker rate, finger tapping rate, syllable presentation rate) [54, 135, 139, 140, 174, 175], (c) comparison of signal locations with macroscopic vessel maps [108, 133, 134, 152, 153] or neuronal activation maps [176–178], and (d) modeling of activation-induced MR signal changes based upon knowledge of MR physics and human cerebral physiology [66, 111–114, 179–181].

EPI lends itself well to many of these contrast mechanism studies since its pulse sequence parameters are easily modulated, and many images can be obtained rapidly with minimal systematic artifacts which can become more problematic with longer image time course acquisition times. Presented below is an example of how EPI can be utilized in the study of fMRI contrast mechanisms.

Relaxation Rate Comparison

As mentioned above, many variables can contribute to the a change in MR signal intensity during brain activation. Among the possible sources of activation-induced MR signal changes are a decrease in $R2^*$ and $R2$, movement near a high signal intensity gradient, a net frequency shift causing a subvoxel spatial shift, an increase in apparent $T1$ relaxation rate caused by perfusion changes, and a possible change in proton density. The extent to which these parameters contribute depends on the pulse sequence parameters and conditions of the experiment.

The degree to which each parameter contributes to the signal intensity change under specific pulse-sequence conditions is a question that is central to a large proportion of contrast mechanism studies. For example, the issue of flow vs. oxygenation contrast entails understanding how much of the signal change (or what areas) are related primarily to oxygenation changes and how much is due to non-susceptibility related flow changes. It is essentially a question of localization, interpretation, and ultimately quantification. The proportion and location of large draining veins vs. capillary contributions affects BOLD contrast. Large draining veins may cause oxygenation-related signal changes far removed from

regions of activation due to the fact that the blood volume in each voxel heavily weights the magnitude of susceptibility-related signal change. Also, large vessels may give artificial "hot spots" that may be misinterpreted as the location of highest neuronal activation. These issues are not yet been fully understood. The study described below demonstrates the manner in which EPI can be used to address such issues.

The study below demonstrates (a) that the predominant mechanism of signal changes with susceptibility-weighted sequences having TR of 1 s or greater is from alterations in transverse relaxation rate due to changes in the susceptibility of hemoglobin during activation and has minimal non-susceptibility-related contributions [108, 109, 116, 164, 165], and (b) the predominant vascular scale contributing to BOLD contrast during brain activation varies significantly over space.

In this study, the assumption was made that the resting and activated MRI signal intensity, S_r and S_a respectively, may be approximated by:

$$S_r = S_{r_0} e^{-(R_{2r} TE)} \quad \text{and} \quad S_a = S_{a_0} e^{-(R_{2a} TE)}$$

Resting and activated signal at $TE = 0$, S_{r_0} and S_{a_0} can be altered by changes in proton density and/or T1. Resting and activated transverse relaxation rates, R_{2r} ($1/T_{2r}$), and R_{2a} ($1/T_{2a}$), can be altered in this context by changes in the magnetic susceptibility of blood, which causes changes in R_2' ($R_2' = R_2 + R_2'$). Temporally and spatially registered time course measurements of R_2 , R_2^* , and S_0 during rest and activation enables accurate separation of these flow (non-susceptibility-related) and oxygenation (susceptibility-related) effects.

Using a combined spin-echo and gradient-echo EPI sequence (SEGE EPI) [165] (Fig. 12), a pair of spin-echo and gradient-echo single-shot echo-planar time course series were collected simultaneously and processed in an identical manner. In Fig. 12 the missing phase-encode blips are incorporated to allow for two line phase correction for each image [182, 183]. SEGE EPI has proven

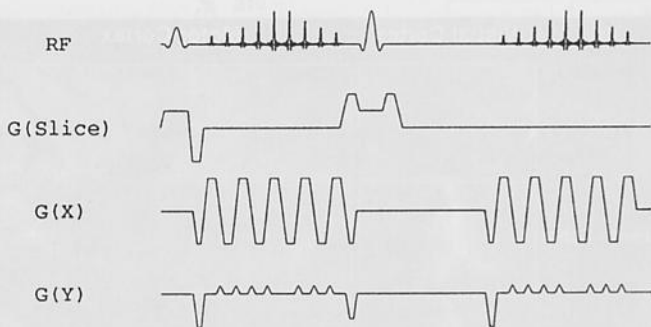
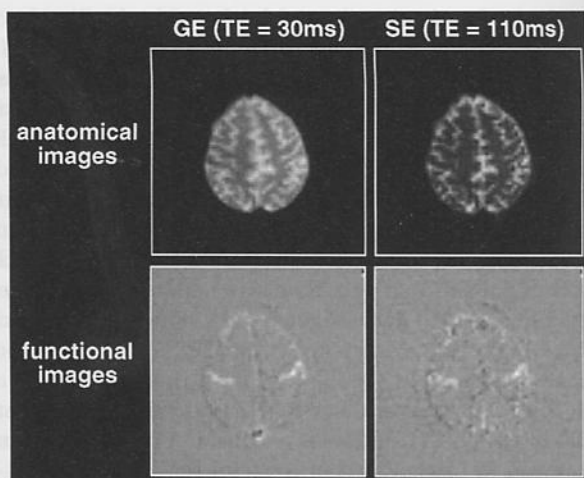


Fig. 12. SEGE-EPI. This sequence allows for the collection of spin-echo (T_2 -weighted) and gradient-echo (T_2^* -weighted) echo planar image pairs within about 50 ms of each other. This sequence is used to obtain spatially and temporally registered gradient-echo and spin-echo time course series for voxelwise comparison of activation-induced signal change dynamics and locations with different contrast weightings. Systematic incrementation of the two TE values in each sequential time course image also enables the simultaneous mapping of relative transverse relaxation rates (R_2^* , R_2 , and R_2') and steady-state magnetizations

Fig. 13. The first pair of anatomical images and the corresponding functional correlation images obtained simultaneously from a SEGE EPI time course series. The gradient-echo functional image (*GE*) appears to have a higher functional CNR than the spin-echo image (*SE*). The signal change locations also show differences



useful for voxel-wise comparisons of relative $R2^*$ and $R2$ contrast [165, 184]. Imaging was performed on a 1.5-T GE Signa scanner using a local three-axis gradient coil and a quadrature transmit/receive birdcage RF coil. Voxel volume was $3.75 \times 3.75 \times 5 \text{ mm}^3$.

The first part of the experiment entailed obtaining SEGE EPI time course series ($TR = 1 \text{ s}$) during cyclic on/off finger movement using single TE values of 30 ms (gradient-echo) and 110 ms (spin-echo). With this protocol the relative signal change latencies can be compared and the relative relaxation rates ($R2^*/R2$) mapped. Figure 13 shows the first pair of anatomical images and the corresponding functional correlation images obtained. The gradient-echo functional image more clearly shows activation-induced signal changes. Also, the signal change locations differ. Figure 14 shows a magnification of motor cortex and

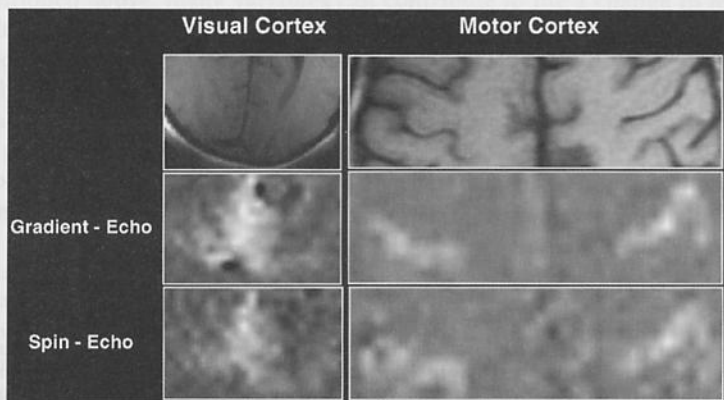


Fig. 14. Magnification of simultaneously obtained and identically processed gradient-echo ($TE = 30 \text{ ms}$) and spin-echo ($TE = 110 \text{ ms}$) functional correlation images of visual and motor cortex activation

visual cortex functional correlation images. Corresponding high-resolution anatomical images are shown for reference. In spin-echo sequences pulsatile and/or large vessel artifacts are significantly reduced at some expense in functional CNR.

Figure 15 shows gradient-echo and spin-echo time course signals from the same motor cortex region of interest obtained simultaneously using the SEGE sequence. The vertical scales are the same to illustrate the relative contrasts typically obtained. To compare the relative latencies of the signal changes each activation/rest cycle was averaged over time and then normalized. This comparison is shown in Fig. 16. A monoexponential model of the signal change onset is an oversimplification of the behavior of the MR signal change on activation, but for the purpose of comparison with the literature values [54], similar monoexponential fits to the initial rise in signal were performed. The fitted onset time constants were 3.67 ± 0.30 s for the gradient-echo sequence and 4.19 ± 0.46 for the spin-echo sequence. Within the certainty of experimental noise the two onset latencies are the same.

As discussed above, mathematical models of the BOLD effect have suggested that the $\Delta R2^*/\Delta R2$ ratio is highly dependent on compartment (red blood cell and vessel) size, activation-induced susceptibility change, and the diffusion coef-

Fig. 15. Simultaneously obtained gradient-echo (GE; TE = 30 ms) and spin-echo (SE; TE = 110 ms) time-course signal from the same region of interest in motor cortex. Vertical scales have the same range to illustrate the relative contrasts. Horizontal bars indicate when bilateral finger tapping was performed

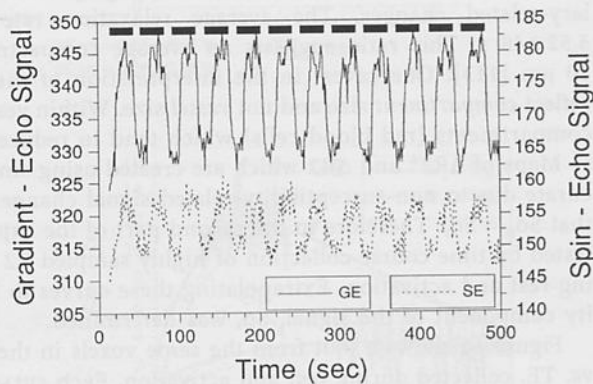


Fig. 16. Normalized gradient-echo and spin-echo time course created by averaging all of the 12 on-off cycles in Fig. 15. The signal change shapes do not show significant differences

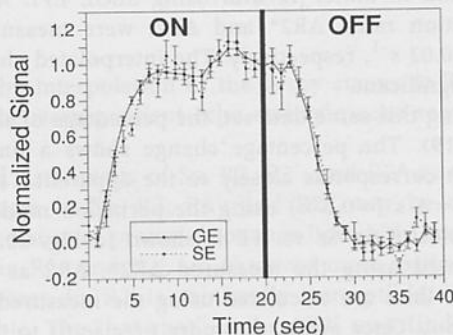
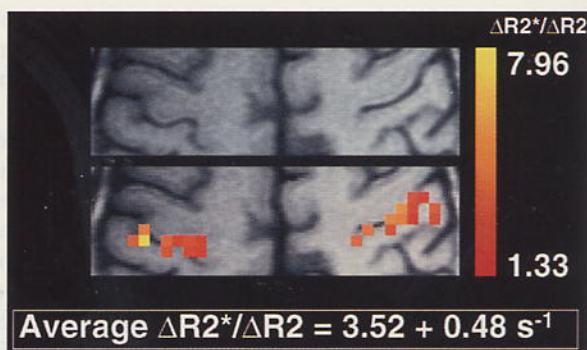


Fig. 17. Relative activation-induced $\Delta R2^*/\Delta R2$ map created from voxels showing activation with both the gradient-echo and spin-echo contrast weightings. The ratio varies considerably in space and has an average value of 3.52 ± 0.48



ficient. The relative change in relaxation rates, [determined by $\Delta R2^*(*) = -\ln(S_a/S_r)$], were compared on a voxelwise basis, in regions showing common activation, directly from the signal changes in the SEGE-EPI time course series. Figure 17 shows the map of $\Delta R2^*/\Delta R2$ values. The variation in $\Delta R2^*/\Delta R2$ values suggests a heterogeneous distribution of predominant vascular scales. The highest ratio is observed directly within a sulcus where a large vessel appears to be. Lower ratios appear to be predominantly within gray matter regions, indicating capillary-related changes. The average relaxation rate ratio was found to be 3.52 ± 0.48 s. This ratio suggests an average compartment size of approximately $10 \mu\text{m}$ [113]. One caveat in the interpretation of these maps is that the ratios reflect *compartment* size and not *vessel* size. Within vessels there are many smaller compartments (red blood cells) which tend to reduce this ratio in large vessels.

Maps of $\Delta R2^*$ and $\Delta R2$ which are created using single TE values may be inaccurate due to non-susceptibility-related signal changes. The assumption is made that $S_{0a} = S_{0r}$. Therefore in the second part of the experiment this assumption is tested by time course collection of highly sampled R2 and R2* decay curves during rest and activation. Extrapolating these curves to TE = 0, the nonsusceptibility component of the signal, S_0 , was determined.

Figure 18 shows a plot from the same voxels in the motor cortex of the $\ln(S)$ vs. TE, collected during rest and activation. Each curve has 100 points (gradient-echo TE = 25–74.5 ms, spin-echo TE = 100–199 ms). All data for this plot were obtained in under 17 min using SEGE EPI. Activation-induced changes in the relaxation rates, $\Delta R2^*$ and $\Delta R2$, were measured to be $-0.81 \pm 0.02 \text{ s}^{-1}$ and $-0.19 \pm 0.02 \text{ s}^{-1}$, respectively. The interpolated change in S_0 using the $\Delta R2^*$ curves was significant.

Using this same data set, the percentage of signal change vs. TE was computed (Fig. 19). The percentage change shows a linear TE dependence. The ΔS_0 at TE = 0 corresponds closely to the apparent T1-related signal changes predicted at TR = 1 s ($\approx 0.6\%$) using the perfusion model of Kwong et al. [54].

A plot of $S_a - S_r$ vs. TE is shown in Fig. 20. Bold lines indicate $S_a - S_r$ values calculated using the measured $\Delta R2^*$, $\Delta R2$ as well as extrapolated ΔS_0 values. Lighter lines are calculated using the measured $\Delta R2^*$, $\Delta R2$ values and assuming $S_{0r} = S_{0a}$. Once again, the more precise fit to the ΔS curve was that which used

Fig. 18. Resting and active R_2 , R_2^* curves obtained simultaneously during rest and activation from identical regions in motor cortex. Each curve has 100 points. Gradient-echo (GE) TE = 25 to 74.5 ms; spin-echo (SE) TE = 100–199 ms). All data for this plot were obtained in under 17 min using SEGE EPI. The observed change in S_0 , when using the ΔR_2^* curves, was significant

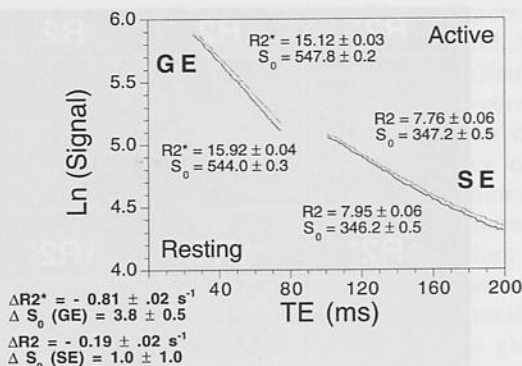


Fig. 19. Percentage of gradient-echo (GE) and spin-echo (SE) signal change vs. TE from the same data set as in Fig. 18. The TE dependence of the fractional signal change appears linear, and the zero intercept shows a positive change with activation

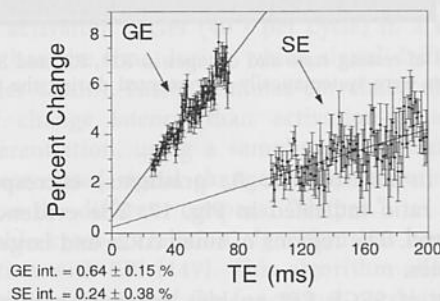
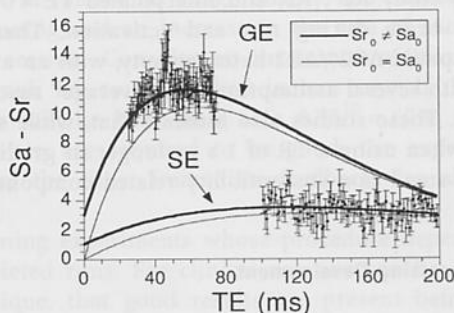


Fig. 20. Signal difference vs. TE from the same data set as in Figs. 18 and 19. **Bold lines** were calculated using the measured resting and active R_2 , R_2^* , and S_0 values; **lighter lines** were calculated using the measured R_2 and R_2^* values and assuming that $S_{a0} = S_{r0}$. The more precise fit to the ΔS curve was that which used the S_{r0} and S_{a0} values obtained by interpolation of the decay curves to TE = 0



the S_{r0} and S_{a0} values obtained by interpolation of the decay curves to TE = 0. The ratio in contrast at TE \approx T2* between gradient-echo and spin-echo sequences is about 3.5–1.

Lastly, using similarly acquired data, maps of S_0 , R_2 , R_2' , and R_2^* as well as maps of activation-induced changes in S_0 , R_2 , R_2' , and R_2^* may be created (Fig. 21). The R_2' maps (direct measure of proton resonance linewidth) were calculated from $R_2^* - R_2$. Decreases in R_2^* and R_2' are observed most easily. Using this method of analysis, a decrease in R_2 is minimally perceptible, and S_0 changes are relatively imperceptible. The "hot spot" in the $\Delta R_2'$ map (indicating

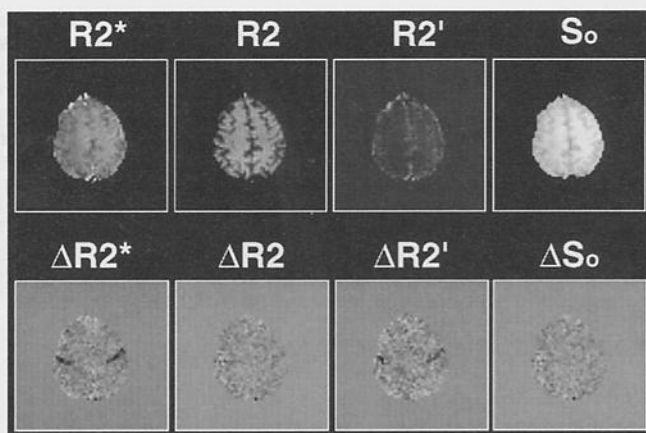


Fig. 21. Maps of resting state and changes in $R2^*$, $R2$, and S_0 , created using SEGE EPI, in which the TE values were systematically incremented during the time-course collection of images

a change in macroscopic B_0 gradients) corresponds closely with the largest $\Delta R2^*/\Delta R2$ ratio indicated in Fig. 17. The evidence indicates that this region is likely a vessel. The regions of small $\Delta R2'$ and larger $\Delta R2$ are likely smaller vessels or capillaries.

The use of SEGE EPI enables acquisition of spatially and temporally registered, high-SNR measurements of $R2^*$ and $R2$ in a reasonable amount of time. In this study $R2^*$, $R2$, and interpolated TE = 0 signal were measured over time in the brain during rest and activation. These studies typically demonstrate large spatial $\Delta R2^*/\Delta R2$ heterogeneity, with an average ratio of about 3.5, indicating, with several assumptions, an "average" susceptibility compartment size of 8–10 μm . These studies also indicate that, while susceptibility effects clearly dominate when using a TR of 1 s or longer in gradient-echo or spin-echo sequences, a very small non-susceptibility-related component contributes.

Postprocessing Development

The challenge of accurately determining regions of significant activation from fMRI data is nontrivial and has yet to be solved. Some of the developments addressing this issue include: (a) the development of accurate and robust motion correction [186, 187] and/or suppression methods, (b) the determination of the noise distribution [120, 121, 155], (c) the determination of the temporal [142] and spatial [187] correlation of activation-induced MR signal changes and of baseline MR signal, (d) the characterization or assessment of the temporal behavior or shape of activation-induced signal changes [136–138, 155, 174], and (e) the characterization of how the above-mentioned factors vary in time, space [133, 134], across tasks [137, 138, 155], and with different pulse sequence parameters [54].

Several of the postprocessing issues may be bypassed or addressed more effectively using the flexibility and rapid image sampling capabilities of EPI. Examples are given of how EPI can aid in the reduction of various manifestations of motion artifacts, including pulsatile, sudden, gradual, and stimulus-correlated motion. First, because the rapid image sampling rate of EPI allows for critical sampling of many problematic noise frequencies, these frequencies can be rejected using simple band stop filters [121]. With single-shot EPI motion effects above the time scale of 40–100 ms are virtually eliminated. Slower motion that occurs between each shot (100 ms, 6 s) cause primarily misregistration. These effects can be reduced by the use of currently available image registration algorithms [185, 186]. In two-dimensional Fourier transform techniques motion on this time scale is manifested not only as misregistration but also as ghosting that is propagated throughout the image [100, 102]. With EPI very slow motion, manifested as a drift in the time course, is reduced simply by the ability to collect a larger number of on/off activation cycles (40 s per cycle) in a single time course whose duration is less than the time during which signal drift manifests itself (five on/off cycles in under 4 min). Lastly, stimulus correlated motion generally has a different signal change latency than activation-induced signal changes. This fact allows differentiation, using a sampling rate of at least one image every 2 s, of stimulus-correlated signal changes from activation-induced signal changes, based simply on the different temporal “shapes.”

Recently a real-time updatable cross-correlation algorithm has been successfully implemented in conjunction with EPI [149]. This algorithm allows images to be continually obtained until the quality of the functional correlation images (updated at a rate of one per second) is suitable. Rapid acquisition of echo-planar images can allow rapid feedback in functional image quality and subsequently a high degree of experimental tuning and an increase in the rate of successful fMRI experiments per imaging session. Consider an investigation (clinical or research) in which different stimuli are to be applied in ten runs. If there is only a 5% chance that one run will be bad, there is a $0.95^{10} = 60\%$ chance that all ten will be good. If all ten are required to be good, the experiment results must be rejected 40% of the time. Immediate feedback can alleviate this problem.

One can also imagine performing experiments whose procedure depends on knowing results from just completed runs. For clinical use one can be sure, if using the real-time fMRI technique, that good results are present before the patient leaves the scanner.

In general, an array of statistical and prestatistical postprocessing methods have been put forward. The statistical methods include the use of *Z* scores [188], analysis of variance [189], split-half *t* test [100, 190], the Kolmogorov-Smirnov test [191], and other nonparametric tests [192]. Prestatistical methods include cross-correlation analysis [101], auto-correlation analysis [167], phase tagging [133, 134, 154, 155], principle-components analysis [193], time-frequency analysis [147], and power-spectrum analysis [101, 120, 121, 194]. Currently no one best postprocessing technique exists, or may ever exist, because of the large number of changing variables which contribute to the activation-induced signal change and underlying noise. The best types of postprocessing methods

are likely to be those that are adaptable to variations (across scans, regions, tasks, and pulse-sequences) in signal and noise characteristics.

Applications

Most studies involving the development of fMRI from a contrast mechanism, pulse-sequence, and postprocessing standpoint have used primary motor and visual cortex activation due to the easily elicited signal changes. Listed below are some of the applications of fMRI that have gone beyond simple finger tapping or visual stimulation. Most of the studies were performed using EPI. The primary auditory cortex [195–201] and the cerebellum [202–204] have been studied using fMRI. Detailed mapping of regions activated in the primary motor cortex [205–208] and visual cortex [154–156, 209, 210] has been performed as well. Subcortical activity has been observed during visual stimulation [167] and finger movement [211]. Activity elicited in the gustatory cortex has also been mapped [212]. Other studies using fMRI have observed organizational differences related to handedness [213]. Activation changes during motor task learning have been observed in the primary motor cortex [214] and cerebellum [215, 216].

Cognitive studies in normal subjects have included word generation [217–219], mental imagery [220, 221], mental rehearsal of motor tasks and complex motor control [211, 222, 223], speech perception [195, 197, 198, 224, 225], single-word semantic processing [197, 198, 224, 225], working memory [226, 227], spatial memory [228], and visual recall [229]. Studies have observed modulation of activity by attention modulation [155].

fMRI has been extremely useful in mapping visual cortex in humans [155, 190, 209, 230–234]. In particular, because of its high image acquisition rate EPI lends itself to the mapping specific types of neuronal activation. The illusion of motion is transiently perceived following particular stimuli. Recently Tootell et al. [233], using EPI with BOLD contrast at 1.5 T, have been able to observe transient activation in MT/V5 elicited by the illusion of motion following stimulation by radially moving concentric rings.

Studies have also been performed involving specific pathologies. Abnormal connectivity of the visual pathways in human albinos has been demonstrated [235]. Changes in organization in the sensorimotor area after brain injury has been observed [236]. One study has demonstrated larger fMRI signal changes, on the average, in schizophrenic patients [237]. The ability to localize seizure activity has also been demonstrated by fMRI [238]. In addition, preliminary data demonstrating the effects of drugs on brain activation have been presented [239]. Activity associated with obsessive-compulsive behavior has also been observed [240, 241].

The immediate potential for clinical application is currently being explored. "Essential" areas of the sensory and motor cortex as well as language centers have been mapped using both fMRI and electrical stimulation techniques [178, 242]. Activity foci observed across the two methods have shown a high spatial correlation, demonstrating the potential for fMRI to compliment or replace the invasive technique in the identification of cortical regions which should be

avoided during surgery. Along this avenue of research fMRI has developed the ability to reliably identify the hemisphere where language functions reside, potentially complimenting or replacing the Wada test (hemisphere specific application of an anesthetic amobarbital) for language localization that is also currently used clinically prior to surgery [243].

Several review articles and chapters on fMRI techniques and applications are currently available [135, 144, 187, 196, 244–248]. In general, the several fMRI research avenues – functional imaging platform development, contrast mechanism research, postprocessing development, and applications – are progressing in a manner that is both complimentary and synergistic. Because of the rigor and creativity of the investigators in this newly created and interdisciplinary field and, in part, because of the robustness of EPI as a functional imaging tool, fMRI is progressing at an accelerating pace.

Acknowledgements. The writing of this chapter benefited from enlightening discussions with Jeffrey Binder, Bharat Biswal, Robert Cox, Ted DeYoe, Victor Haughton, James Hyde, Andrej Jesmanowicz, Stephen Rao, Allen Song, Elliot Stein, and Steven Tan from the Medical College of Wisconsin; and John Baker, Jack Belliveau, Jerry Boxerman, Timothy Davis, Kathleen Donahue, Ken Kwong, Bruce Rosen, Robert Savoy, Roger Tootell, and Robert Weisskoff from the Massachusetts General Hospital. Thanks also to Steven Tan for providing the interleaved echo-planar images.

References

1. Mansfield P (1977) Multi-planar image formation using NMR spin echoes. *J Phys C10*:L55–L58
2. Stehling MK, Turner R, Mansfield P (1991) Echo-planar imaging: magnetic resonance imaging in a fraction of a second. *Science* 254:43–50
3. Edelman R, Wielopolski P, Schmitt F (1994) Echo-planar MR imaging. *Radiology* 192:600–612
4. Cohen MS, Weisskoff RM (1991) Ultra-fast imaging. *Magn Reson Imaging* 9:1–37
5. Mansfield P, Morris PG (1982) *NMR imaging in biomedicine*. Academic, New York
6. Roland PE (1993) *Brain activation*. Wiley-Liss, New York
7. Churchland PS, Sejnowski TJ (1992) *The computational brain*. MIT Press, Cambridge
8. Kuffler SW, Nicholls JG, Martin AR (1984) *From neuron to brain*. Sinauer Associates, Sunderland
9. Krnjevic K (1975) Coupling of neuronal metabolism and electrical activity. In: Ingvar DH, Lassen NA (eds) *Brain work*. Munksgaard, Copenhagen, p 65
10. Hillyard SG, Picton TW (1987) In: *Handbook of physiology, section 1: neurophysiology*. American Physiological Society, New York, p 519
11. Hari R (1991) On brain's magnetic responses to sensory stimuli. *J Clin Neurophysiol* 8:157–169
12. Kaufman L, Williamson SJ (1982) Magnetic location of cortical activity. *Ann N Y Acad Sci* 388:197–213
13. Prichard J, Rothman D, Novotny E, Petroff O, Kuwabara T, Avison M, Howsman A, Hanstock C, Shulman R (1991) Lactate rise detected by ¹H NMR in human visual cortex during physiologic stimulation. *Proc Natl Acad Sci USA* 88:5829–5831
14. Merboldt K-D, Bruhn H, Hanicke W, Michaelis T, Frahm J, (1992) Decrease of glucose in the human visual cortex during photic stimulation. *Magn Reson Med* 25:187–194
15. Fox PT, Raichle ME, Mintun MA, Dence C (1988) Nonoxidative glucose consumption during focal physiologic neural activity. *Science* 241:462
16. Phelps ME, Kuhl DE, Mazziotta JC (1981) Metabolic mapping of the brain's response to visual stimulation: studies in humans. *Science* 211:1445–1448
17. Mazziotta JC, Phelps ME (1985) Human neuropsychological imaging studies of local brain metabolism: strategies and results. In: Sokoloff L (ed) *Brain imaging and brain function*. Raven, New York, p 121

18. Haxby JL, Grady CL, Ungerleider LG, Horowitz B (1991) Mapping the functional neuroanatomy of the intact human brain with brain work imaging. *Neuropsychologia* 29:539-555
19. Roy CS, Sherrington CS (1890) On the regulation of the blood-supply of the brain. *J Physiol* 11:85-108
20. Gotoh F, Tanaka K (1987) In: Vinken PJ, Bruyn GW, Klawans HL (eds) *Handbook of clinical neurology*. Elsevier Science, New York, p 47
21. Kushinsky W (1982/1983) Coupling between functional activity, metabolism, and blood flow in the brain: state of the art. *Microcirculation* 2:357-378
22. Busija DW, Heistad DD (1984) Factors involved in the physiological regulation of the cerebral circulation. Springer, Berlin Heidelberg New York
23. Ursino M (1991) Mechanisms of cerebral blood flow regulation. *Crit Rev Biomed Eng* 18:255-288
24. Lou HC, Edvinsson L, MacKenzie ET (1987) The concept of coupling blood flow to brain function: revision required? *Ann Neurol* 22:289-297
25. Kushinsky W (1991) Physiology of cerebral blood flow and metabolism. *Arzneimittelforschung* 41:284-288
26. Moskalenko YE, Weinstein GB, Demchenko IT, Kislyakov YY, Krivchenko AI (1980) Biophysical aspects of cerebral circulation. Pergamon, Oxford
27. Estrada C, Mengual E, Gonzalez C (1993) Local NADPH-diaphorase neurons innervate pial arteries and lie close or project to intracerebral blood vessels: a possible role for nitric oxide in the regulation of cerebral blood flow. *J Cereb Blood Flow Metab* 13:978-984
28. Dirnagl U, Lindauer U, Villringer A (1993) Role of nitric oxide in the coupling of cerebral blood flow to neuronal activation in rats. *Neuroscience Lett* 149:43-46
29. Iadecola C (1993) Regulation of cerebral microcirculation during neural activity: is nitric oxide the missing link? *Trends Neurosci* 16:206-214
30. Mchedlishvili G (1986) Arterial behavior and blood circulation in the brain. Plenum, New York
31. Ingvar DH (1975) In: Ingvar DH, Lassen NA (eds) *Brain work*. Munksgaard, Copenhagen, p 397
32. Grafton ST, Woods RP, Mazziotta JC, Phelps ME (1991) Somatotopic mapping of the primary motor cortex in humans: activation studies with cerebral blood flow and positron emission tomography. *J Neurophysiol* 66:735-743
33. Colebatch JG, Deiber M-P, Passingham RE, Friston KJ, Frackowiack RSJ (1991) Regional cerebral blood flow during voluntary arm and hand movements in human subjects. *J Neurophysiol* 65:1392-1401
34. Fox PT, Raichle ME (1985) Stimulus rate determines regional brain blood flow in striate cortex. *Ann Neurol* 17:303-305
35. Fox PT, Raichle ME (1991) Stimulus rate dependence of regional cerebral blood flow in human striate cortex, demonstrated by positron emission tomography. *J Neurophysiol* 51:1109-1120
36. Cameron OG, Modell JG, Hichwa RD, Agranoff BW, Koeppe RA (1990) Changes in sensory-cognitive input: effects on cerebral blood flow. *J Cereb Blood Flow Metab* 10:38-42
37. Sandman CA, O'Halloran JP, Isenhardt R (1984) Is there an evoked vascular response? *Science* 224:1355-1356
38. Belliveau JW, Kennedy DN, McKinstry RC, Buchbinder BR, Weisskoff RM, Cohen MS, Vevea JM, Brady TJ, Rosen BR (1991) Functional mapping of the human visual cortex by magnetic resonance imaging. *Science* 254:716-719
39. Villringer A, Planck J, Hock C, Scheinkofer L, Dirnagl U (1993) Near infrared spectroscopy (NIRS): a new tool to study hemodynamic changes during activation of brain function in human adults. *Neurosci Lett* 154:101-104
40. Fox PT, Raichle ME (1986) Focal physiological uncoupling of cerebral blood flow and oxidative metabolism during somatosensory stimulation in human subjects. *Proc Natl Acad Sci USA* 83:1140-1144
41. Frostig RD, Lieke EE, Ts'o DY, Grinvald A (1990) Cortical functional architecture and local coupling between neuronal activity and the microcirculation revealed by in vivo high-resolution optical imaging of intrinsic signals. *Proc Natl Acad Sci USA* 87:6082-6086
42. Grinvald A, Frostig RD, Siegel RM, Bratfeld E (1991) High-resolution optical imaging of functional brain architecture in the awake monkey. *Proc Natl Acad Sci USA* 88:11559-11563
43. Frostig RD (1994) What does in vivo optical imaging tell us about the primary visual cortex in primates? In: Peters A, Rockland KS (eds) *Cerebral cortex*, vol 10. Plenum, New York, p 331

44. Rosen BR, Belliveau JW, Chien D (1989) Perfusion imaging by nuclear magnetic resonance. *Magn Reson Q* 5:263-281
45. Rosen BR, Belliveau JW, Vevea JM, Brady TJ (1990) Perfusion imaging with NMR contrast agents. *Magn Reson Med* 14:249-265
46. Belliveau JW, Rosen BR, Kantor HL, Rzedzian RR, Kennedy DN, McKinstry RC, Vevea JM, Cohen MS, Pykett IL, Brady TJ (1990) Functional cerebral imaging by susceptibility-contrast NMR. *Magn Reson Med* 14:538-546
47. Rosen BR, Belliveau JW, Aronen HJ, Kennedy D, Buchbinder BR, Fischman A, Gruber M, Glas J, Weisskoff RM, Cohen MS, Hochberg FH, Brady TJ (1991) Susceptibility contrast imaging of cerebral blood volume: human experience. *Magn Reson Med* 22:293-299
48. Villringer A, Rosen BR, Belliveau JW, Ackerman JL, Lauffer RM, Buxton RB, Chao Y-S, Wedeen VJ, Brady TJ (1988) Dynamic imaging with lanthanide chelates in normal brain: contrast due to magnetic susceptibility effects. *Magn Reson Med* 6:164-174
49. Moonen CT, Liu G, van Gelderen P, Sobering G (1992) A fast gradient-recalled MRI technique with increased sensitivity to dynamic susceptibility effects. *Magn Reson Med* 26:184-189
50. Moonen CTW, van Zijl PCM, Frank JA, LeBihan D, Becker ED (1990) Functional magnetic resonance imaging in medicine and physiology. *Science* 250:53-61
51. Williams DS, Detre JA, Leigh JS, Koretsky AS (1992) Magnetic resonance imaging of perfusion using spin-inversion of arterial water. *Proc Natl Acad Sci USA* 89:212-216
52. Detre JA, Leigh JS, Williams DS, Koretsky AP (1992) Perfusion imaging. *Magn Reson Med* 23:37-45
53. Edelman RR, Sievert B, Wielopolski P, Pearlman J, Warach S (1994) Noninvasive mapping of cerebral perfusion by using EPSTAR MR angiography. *JMRI* 4(P):68 (abstract)
54. Kwong KK, Belliveau JW, Chesler DA, Goldberg IE, Weisskoff RM, Poncelet BP, Kennedy DN, Hoppel BE, Cohen MS, Turner R, Cheng HM, Brady TJ, Rosen BR (1992) Dynamic magnetic resonance imaging of human brain activity during primary sensory stimulation. *Proc Natl Acad Sci USA* 89:5675-5679
55. Stehling MK, Schmitt F, Ladebeck R (1993) Echo-planar MR imaging of human brain oxygenation changes. *JMRI* 3:471-474
56. Bandettini PA, Wong EC, Hinks RS, Tikofsky RS, Hyde JS (1992) Time course EPI of human brain function during task activation. *Magn Reson Med* 25:390-397
57. Blamire AM, Ogawa S, Ugurbil K, Rothman D, McCarthy G, Ellermann JM, Hyder F, Rattner Z, Shulman RG (1992) Dynamic mapping of the human visual cortex by high-speed magnetic resonance imaging. *Proc Natl Acad Sci USA* 89:11069-11073
58. Frahm J, Bruhn H, Merboldt K-D, Hancic W, Math D (1992) Dynamic MR imaging of human brain oxygenation during rest and photic stimulation. *JMRI* 2:501-505
59. Ogawa S, Lee T-M, Nayak AS, Glynn P (1990) Oxygenation-sensitive contrast in magnetic resonance image of rodent brain at high magnetic fields. *Magn Reson Med* 14:68-78
60. Ogawa S, Lee T-M (1990) Magnetic resonance imaging of blood vessels at high fields: in vivo and in vitro measurements and image simulation. *Magn Reson Med* 16:9-18
61. Ogawa S, Lee TM, Kay AR, Tank DW (1990) Brain magnetic resonance imaging with contrast dependent on blood oxygenation. *Proc Natl Acad Sci USA* 87:9868-9872
62. Ogawa S, Tank DW, Menon R, Ellermann JM, Kim S-G, Merkle H, Ugurbil K (1992) Intrinsic signal changes accompanying sensory stimulation: functional brain mapping with magnetic resonance imaging. *Proc Natl Acad Sci USA* 89:5951-5955
63. Turner R, LeBihan D, Moonen CTW, Despres D, Frank J (1991) Echo-planar time course MRI of cat brain oxygenation changes. *Magn Reson Med* 27:159-166
64. Turner R, Jezzard P, Wen H, Kwong KK, Bihan DL, Zeffiro T, Balaban RS (1993) Functional mapping of the human visual cortex at 4 and 1.5 tesla using deoxygenation contrast EPI. *Magn Reson Med* 29:277-279
65. Jezzard P, Heinmann F, Taylor J, Despres D, Wen H, Balaban RS, Turner R (1994) Comparison of EPI gradient-echo contrast changes in cat brain caused by respiratory challenges with direct simultaneous evaluation of cerebral oxygenation via a cranial window. *NMR Biomed* 7:35-44
66. Weisskoff RM, Zuo CS, Boxerman JL, Rosen BR (1994) Microscopic susceptibility variation and transverse relaxation: theory and experiment. *Magn Reson Med* 31:601-610
67. Edelman RR, Mattle HP, Atkinson DJ, Hoogewood HM, (1990) MR angiography. *AJR* 154:937-946
68. Listerud J (1991) First principles of magnetic resonance angiography. *Magn Reson Q* 7:136-170

69. LeBihan D, Breton E, Lallemand D, Aubin M-L, Vignaud J, Laval-Jeantet M (1988) Separation of diffusion and perfusion in intravoxel incoherent motion MR imaging. *Radiology* 168:497-505
70. LeBihan D (1990) Magnetic resonance imaging of perfusion. *Magn Reson Med* 14:283-292
71. LeBihan D, Turner R, Moonen CT, Pekar J (1991) Imaging of diffusion and microcirculation with gradient sensitization: design, strategy, and significance. *JMRI* 1:7-28
72. LeBihan D (1992) Theoretical principles of perfusion imaging: applications to magnetic resonance imaging. *Invest Radiol* 27:S6-S11
73. Kwong KK, McKinstry RC, Chien D, Crawley AB, Pearlman JD, Rosen BR (1991) CSF-suppressed quantitative single-shot diffusion imaging. *Magn Reson Med* 21:157-163
74. J Pekar, C. T. Moonen, P. C. van Zijl, On the precision of diffusion/perfusion imaging by gradient sensitization. *Magn Reson Med* 23:122-129 (1992)
75. Edelman RR, Siewert B, Adamis M, Gaa J, Laub GP, Wielopolski P (1994) Signal targeting with alternating radiofrequency (STAR) sequences: application to MR angiography. *Magn Reson Med* 31:233-238
76. Pauling L, Coryell CD (1936) The magnetic properties and structure of hemoglobin, oxyhemoglobin, and carbonmonoxyhemoglobin. *Proc Natl Acad Sci USA* 22:210-216
77. Weisskoff RW, Kiihne S (1992) MRI susceptometry: image-based measurement of absolute susceptibility of MR contrast agents and human blood. *Magn Reson Med* 24:375-383
78. Schenck JF (1992) Health and physiological effects of human exposure to whole-body fourtesla magnetic fields during MRI. *Ann N Y Acad Sci* 649:285-301
79. Thulborn KR, Waterton JC, Matthews PM, Radda GK (1982) Oxygenation dependence of the transverse relaxation time of water protons in whole blood at high field. *Biochim Biophys Acta* 714:265-270
80. Brindle KM, Brown FF, Campbell ID, Grathwohl C, Kuchell PW (1979) Application of spin-echo nuclear magnetic resonance to whole-cell systems. *Biochem J* 180:37-44
81. Brooks RA, Chiro GD (1987) Magnetic resonance imaging of stationary blood: a review. *Med Phys* 14:903-913
82. Gomori JM, Grossman RJ, Yu-IP C, Asakura T (1987) NMR relaxation times of blood: dependence on field strength, oxidation state, and cell integrity. *J Comput Assist Tomogr* 11:684-690
83. Matwiyoff NA, Gasparovic C, Mazurchuk R, Matwiyoff G (1990) The line shapes of the water proton resonances of red blood cells containing carbonyl hemoglobin, deoxyhemoglobin, and methemoglobin: implications for the interpretation of proton MRI at 1.5 T and below. *Magn Reson Imag* 8:295-301
84. Hayman LA, Ford JJ, Taber KH, Saleem A, Round ME, Bryan RN (1988) T2 effects of hemoglobin concentration: assessment with in vitro MR spectroscopy. *Magn Reson Imag* 168:489-491
85. Janick PA, Hackney DB, Grossman RI, Asakura T (1991) MR imaging of various oxidation states of intracellular and extracellular hemoglobin. *AJNR* 12:891-897
86. Wright GA, Nishimura DG, Macovski A (1991) Flow-independent magnetic resonance projection angiography. *Magn Reson Med* 17:126-140
87. Wright GA, Hu BS, Macovski A (1991) Estimating oxygen saturation of blood in vivo with MR imaging at 1.5 T. *JMRI* 1:275-283
88. Thulborn KR, Brady TJ (1989) Iron in magnetic resonance imaging of cerebral hemorrhage. *Magn Reson Q* 5:23-38
89. Hoppel BE, Weisskoff RM, Thulborn KR, Moore JB, Kwong KK, Rosen BR (1993) Measurement of regional blood oxygenation and cerebral hemodynamics. *Magn Reson Med* 30:715-723
90. Gilles P, Peto S, Moiny F, Mispelter J, Cuenod C-A (1995) Proton transverse nuclear magnetic relation in oxidized blood: a numerical approach. *Magn Reson Med* 33:93-100
91. Brady TJ (1991) Future prospects for MR imaging. In: Proceedings of the SMRM, 10th annual meeting, San Francisco, p 2
92. Farzaneh F, Riederer SJ, Pelc NJ (1990) Analysis of T2 limitations and off-resonance effects in spatial resolution and artifacts in echo-planar imaging. *Magn Reson Med* 14:123-139
93. Wong EC, Bandettini PA, Hyde JS (1992) Echo-planar imaging of the human brain using a three axis local gradient coil. In: Proceedings of the SMRM, 11th annual meeting, Berlin, p 105
94. Wong EC, Jesmanowicz A, Hyde JS (1991) Coil optimization for MRI by conjugate gradient descent. *Magn Reson Med* 21:39-48
95. Turner R (1993) Gradient coil design: a review of methods. *Magn Reson Imag* 11:903-920

96. Blamire AM, Shulman RG (1994) Implementation of echo-planar imaging on an unmodified spectrometer at 2.1 tesla for functional imaging. *Magn Reson Imag* 12:669-671
97. Jesmanowicz A, Wong EC, DeYoe EA, Hyde JS (1992) Method to correct anatomic distortion in echo-planar images. In: *Proceedings of the SMRM, 11th annual meeting, Berlin*, p 4260
98. Jezzard P, Balaban R (1995) Correction for geometric distortion in echo planar images from B_0 field distortions. *Magn Reson Med* 34:65-73
99. Weisskoff RM, Davis TL (1992) Correcting gross distortion on echo planar images. In: *Proceedings of the SMRM, 11th annual meeting, Berlin*, p 4515
100. Noll DC, Cohen JD, Meyer CH, Schneider W (1995) Spiral k-space MR imaging of cortical activation. *JMRI* 5:49-56
101. Bandettini PA, Jesmanowicz A, Wong EC, Hyde JS (1993) Processing strategies for time-course data sets in functional MRI of the human brain. *Magn Reson Med* 30:161-173
102. Glover GH, Lee AT, Meyers CH (1993) Motion artifacts in fMRI: comparison of 2DFT with PR and spiral scan methods. In: *Proceedings of the SMRM, 12th annual meeting, New York*, p 197
103. Stehling M, Fang M, Ladebeck R, Schmitt F (1992) Functional echo-planar MR imaging at 1 T. *JMRI* 2(P):76 (abstract)
104. Kwong KK, Belliveau JW, Stern CE, Chesler DA, Goldberg IE, Poncelet BP, Kennedy DN, Weisskoff RM, Cohen MS, Turner R, Cheng H-M, Brady TJ, Rosen BR (1992) Functional MR imaging of primary visual and motor cortex. *JMRI* 2(P):76 (abstract)
105. Bandettini PA, Wong EC, Tikofsky RS, Hinks RS, Hyde JS (1992) Echo-planar imaging of cerebral capillary percent deoxyhemoglobin change on task activation. *JMRI* 2(P):76 (abstract)
106. Jesmanowicz A, Bandettini PA, Wong EC, Tan G, Hyde JS (1993) Spin-echo and gradient-echo EPI of human brain function at 3 tesla. In: *Proceedings of the SMRM, 12th annual meeting, New York*, p 1390
107. Frahm J, Merboldt K-D, Hanicke W (1993) Functional MRI of human brain activation at high spatial resolution. *Magn Reson Med* 29:139-144
108. Menon RS, Ogawa S, Tank DW, Ugurbil K (1993) 4 tesla gradient recalled echo characteristics of photic stimulation-induced signal changes in the human primary visual cortex. *Magn Reson Med* 30:380-386
109. Bandettini PA, Wong EC, Jesmanowicz A, Hinks RS, Hyde JS (1994) Spin-echo and gradient-echo EPI of human brain activation using BOLD contrast: a comparative study at 1.5 tesla. *NMR Biomed* 7:12-19
110. Weisskoff RM, Boxerman JL, Zuo CS, Rosen BR (1993) Functional MRI of the brain. *Society of Magnetic Resonance in Medicine, Berkeley*, p 103
111. Kennan RP, Zhong J, Gore JC (1994) Intravascular susceptibility contrast mechanisms in tissues. *Magn Reson Med* 31:9-21
112. Fisel CR, Ackerman JL, Buxton RB, Garrido L, Belliveau JW, Rosen BR, Brady TJ (1991) MR contrast due to microscopically heterogeneous magnetic susceptibility: numerical simulations and applications to cerebral physiology. *Magn Reson Med* 17:336-347
113. Ogawa S, Menon RS, Tank DW, Kim S-G, Merkle H, Ellerman JM, Ugurbil K (1993) Functional brain mapping by blood oxygenation level-dependent contrast magnetic resonance imaging: a comparison of signal characteristics with a biophysical model. *Biophys J* 64:803-812
114. Boxerman JL, Weisskoff RM, Hoppel BE, Rosen BR (1993) MR contrast due to microscopically heterogeneous magnetic susceptibility: cylindrical geometry. In: *Proceedings of the SMRM, 12th annual meeting, New York*, p 389
115. Ugurbil K, Garwood M, Ellermann J, Hendrich K, Hinke R, Hu X, Kim S-G, Menon R, Merkle H, Ogawa S, Salmi R (1993) Imaging at high magnetic fields: initial experiences at 4 T. *Magn Reson Q* 9:259-277
116. Bandettini PA, Wong EC, Jesmanowicz A, Prost R, Cox RW, Hinks RS, Hyde JS (1994) MRI of human brain activation at 0.5 T, 1.5 T, and 3 T: comparisons of $\Delta R2^*$ and functional contrast to noise ratio. In: *Proceedings of the SMR, 2nd annual meeting, San Francisco*, p 434
117. Menon RS, Ogawa S, Strupp JP, Anderson P, Ugurbil K (1995) BOLD based functional MRI at 4 tesla includes a capillary bed contribution: echo-planar imaging mirrors previous optical imaging using intrinsic signals. *Magn Reson Med* 33:453-459
118. Menon RS, Hu X, Anderson P, Ugurbil K, Ogawa S (1994) Cerebral oxy/deoxy hemoglobin changes during neural activation: MRI timecourse correlates to optical reflectance measurements. In: *Proceedings of the SMR, 2nd annual meeting, San Francisco*, p 68

119. Poncelet B, Wedeen VJ, Weisskoff RM, Cohen MS (1992) Measurement of brain parenchyma motion with cine echo-planar MRI. In: Proceedings of the SMRM, 11th annual meeting, Berlin, p 809
120. Weisskoff RM, Baker J, Belliveau J, Davis TL, Kwong KK, Cohen MS, Rosen BR (1993) Power spectrum analysis of functionally-weighted MR data: what's in the noise? In: Proceedings of the SMRM, 12th annual meeting, New York, p 7
121. Jezzard P, LeBihan D, Cuenod C, Pannier L, Prinster A, Turner R (1993) An investigation of the contributions of physiological noise in human functional MRI studies at 1.5 tesla and 4 tesla. In: Proceedings of the SMRM, 12th annual meeting, New York, p 1392
122. Biswal B, DeYoe EA, Jesmanowicz A, Hyde JS (1994) Removal of physiological fluctuations from functional MRI signals. In: Proceedings of the SMR, 2nd annual meeting, San Francisco, p 653
123. Feinberg DA, Mark AS (1987) Human brain motion and cerebrospinal fluid circulation demonstrated with MR velocity imaging. *Radiology* 163:793-799
124. Hajnal JV, Myers R, Oatridge A, Schwieso JE, Young IR, Bydder GM (1994) Artifacts due to stimulus correlated motion in functional imaging of the brain. *Magn Reson Med* 31:283-291
125. Golanov EV, Yamamoto S, Reis DJ (1994) Spontaneous waves of cerebral blood flow associated with a pattern of electrocortical activity. *Am J Physiol* 266:R204-R214
126. Hudetz AG, Roman RJ, Harder DR (1992) Spontaneous flow oscillations in the cerebral cortex during acute changes in mean arterial pressure. *J Cereb Blood Flow Metab* 12:491-499
127. Butts K, Riederer SJ (1992) Analysis of flow effects in echo-planar imaging. *JMRI* 2:285-293
128. Baker JR, Hoppel BE, Stern CE, Kwong KK, Weisskoff RM, Rosen BR (1993) Dynamic functional imaging of the complete human cortex using gradient-echo and asymmetric spin-echo echo-planar magnetic resonance imaging. In: Proceedings of the SMRM, 12th annual meeting, New York, p 1400
129. Frank LR, Stout JC, Archibald S, Buxton RB (1993) Oblique flow compensation for improved functional imaging. In: Proceedings of the SMRM, 12th annual meeting, New York, p 1375
130. Hu X, Kim S-G (1994) Reduction of signal fluctuations in functional MRI using navigator echoes. *Magn Reson Med* 31:495-503
131. Wong EC, Boskamp E, Hyde JS (1992) A volume optimized quadrature elliptical endcap birdcage brain coil. In: Proceedings of the SMRM, 11th annual meeting, Berlin, p 4015
132. Wong EC, Tan G, Hyde JS (1993) A quadrature transmit-receive endcapped birdcage coil for imaging of the human head at 125 MHz. In: Proceedings of the SMRM, 12th annual meeting, New York, p 1344
133. Lee AT, Glover GH, Meyer CH (1995) Discrimination of large venous vessels in time-course spiral blood-oxygen-level-dependent magnetic-resonance functional neuroimaging. *Magn Reson Med* 33:745-754
134. Lee AT, Meyer CH, Glover GH (1993) Discrimination of large veins in time-course functional neuroimaging with spiral k-space trajectories. *JMRI* 3(P):59-60 (abstract)
135. Bandettini PA, Wong EC, Binder JR, Rao SM, Jesmanowicz A, Aaron EA, Lowry TF, Forster HV, Hinks RS, Hyde JS (1995) Functional MRI using the BOLD approach: dynamic characteristics and data analysis methods. In: LeBihan D (ed) *Perfusion and diffusion imaging: MRI*. Raven, New York, pp 335-349
136. Binder JR, Jesmanowicz A, Rao SM, Bandettini PA, Hammeke TA, Hyde JS (1993) Analysis of phase differences in periodic functional MRI activation data. In: Proceedings of the SMRM, 12th annual meeting, New York, p 1383
137. Binder JR, Rao SM, Hammeke TA, Bandettini PA, Jesmanowicz A, Frost JA, Wong EC, Haughton VM, Hyde JS (1993) Temporal characteristics of functional magnetic resonance signal changes in lateral frontal and auditory cortex. In: Proceedings of the SMRM, 12th annual meeting, New York, p 5
138. DeYoe EA, Neitz J, Bandettini PA, Wong EC, Hyde JS (1992) Time course of event-related MR signal enhancement in visual and motor cortex. In: Proceedings of the SMRM, 11th annual meeting, Berlin, p 1824
139. Bandettini PA, Wong EC, Yoe EAD, Binder JR, Rao SM, Birzer D, Estkowski LD, Jesmanowicz A, Hinks RS, Hyde JS (1993) The functional dynamics of blood oxygen level dependent contrast in the motor cortex. In: Proceedings of the SMRM, 12th annual meeting, New York, p 1382
140. Bandettini PA (1993) Functional MRI of the brain. *Society of Magnetic Resonance in Medicine*, Berkeley, p 143

141. Belliveau JW, Kwong KK, Kennedy DN, Baker JR, Benson R, Chesler DA, Weisskoff RM, Cohen MS, Tootell RBH, Fox PT, Brady TJ, Rosen BR (1992) Magnetic resonance imaging mapping of brain function: human visual cortex. *Invest Radiol* 27:S59-S65
142. Friston KJ, Jezzard P, Turner R (1994) Analysis of functional MRI time-series. *Human Brain Mapping* 1:153-171
144. Savoy RL, O'Craven KM, Weisskoff RM, Davis TL, Baker J, Rosen B (1994) Exploring the temporal boundaries of fMRI: measuring responses to very brief visual stimuli. In: *Book of abstracts, Society for Neuroscience, 24th annual meeting, Miami*, p 1264
144. Orrison WW, Lewine JD, Sanders JA, Hartshorne MF (1995) *Functional brain imaging*. Mosby Year Book, St Louis
145. Ives JR, Warach S, Schmitt F, Edelman RR, Schomer DL (1993) Monitoring the patient's EEG during echo planar MRI. *EEG Clin Neurophys* 87:417-420
146. Ernst T, Hennig J (1994) Observation of a fast response in functional MR. *Magn Reson Med* 32:146-149
147. Biswal B, Bandettini PA, Jesmanowicz A, Hyde JS (1993) Time-frequency analysis of functional EPI time-course series. In: *Proceedings of the SMRM, 12th annual meeting, New York*, p 722
148. Song AW, Wong EC, Hyde JS (1994) Echo-volume imaging. *Magn Reson Med* 32:668-671
149. Cox RW, Jesmanowicz A, Hyde JS (1995) Real-time functional magnetic resonance imaging. *Magn Reson Med* 33:230-236
150. Turner R, Jezzard P, Bihan DL, Prinster A (1993) Contrast mechanisms and vessel size effects in BOLD contrast functional neuroimaging. In: *Proceedings of the SMRM, 12th annual meeting, New York*, p 173
151. Frahm J, Merboldt K-D, Hancic W, Kleinschmidt A, Boecker H (1994) Brain or vein-oxygenation or flow? On signal physiology in functional MRI of human brain activation. *NMR Biomed* 7:45-53
152. Haacke EM, Hopkins A, Lai S, Buckley P, Friedman L, Meltzer H, Hedera P, Friedland R, Thompson L, Detterman D, Tkach J, Lewin JS (1994) 2D and 3D high resolution gradient-echo functional imaging of the brain: venous contributions to signal in motor cortex studies. *NMR Biomed* 7:54-62
153. Lai S, Hopkins AL, Haacke EM, Li D, Wasserman BA, Buckley P, Friedman L, Meltzer H, Hedera P, Friedland R (1993) Identification of vascular structures as a major source of signal contrast in high resolution 2D and 3D functional activation imaging of the motor cortex at 1.5T: preliminary results. *Magn Reson Med* 30:387-392
154. Engel SA, Rumelhart DE, Wandell BA, Lee AT, Glover GH, Chichilnisky EJ, Shadlen MN (1994) fMRI of human visual cortex. *Nature* 369:370 [erratum], 525:106 [erratum]
155. DeYoe EA, Bandettini P, Neitz J, Miller D, Winans P (1994) Methods for functional magnetic resonance imaging (fMRI) of the human brain. *J Neurosci Methods* 54:171-187
156. Schneider W, Noll DC, Cohen JD (1993) Functional topographic mapping of the cortical ribbon in human vision with conventional MRI scanners. *Nature* 365:150-153
157. Butts K, Riederer SJ, Ehman RL, Thompson RM, Jack CR (1994) Interleaved echo planar imaging on a standard MRI system. *Magn Reson Med* 31:67-72
158. McKinnon GC (1993) Ultrafast interleaved gradient-echo-planar imaging on a standard scanner. *Magn Reson Med* 30:609-616
159. Duyn JH, Moonen CTW, vanYperen GH, de Boer RW, Luyten PR (1994) Inflow versus deoxyhemoglobin effects in BOLD functional MRI using gradient-echoes at 1.5 T. *NMR Biomed* 7:83-88
160. Boxerman JL, Bandettini PA, Kwong KK, Baker JR, Davis TL, Rosen BR, Weisskoff RM (1995) The intravascular contribution to fMRI signal change: Monte Carlo modeling and diffusion-weighted studies in vivo. *Magn Reson Med* 34:4-10
161. Song AW, Wong EC, Bandettini PA, Hyde JS (1994) The effect of diffusion weighting on task-induced functional MRI. In: *Proceedings of the SMR, 2nd annual meeting, San Francisco*, p 643
162. Boxerman JL, Weisskoff RM, Kwong KK, Davis TL, Rosen BR (1994) The intravascular contribution to fMRI signal change. Modeling and diffusion-weighted in vivo studies. In: *Proceedings of the SMR, 2nd annual meeting, San Francisco*, p 619
163. Menon RS, Hu X, Adriany G, Anderson P, Ogawa S, Ugurbil K (1994) Comparison of spin-echo EPI, asymmetric spin-echo EPI and conventional EPI applied to functional neuroimaging. The effect of flow crushing gradients on the BOLD signal. In: *Proceedings of the SMR, 2nd annual meeting, San Francisco*, p 622

164. Bandettini PA, Wong EC, Hinks RS, Estkowski L, Hyde JS (1992) Quantification of changes in relaxation rates $R2^*$ and $R2$ in activated brain tissue. In: Proceedings of the SMRM, 11th annual meeting, Berlin, p 719
165. Bandettini PA, Wong EC, Jesmanowicz A, Hinks RS, Hyde JS (1993) Simultaneous mapping of activation-induced $\Delta R2^*$ and $\Delta R2$ in the human brain using a combined gradient-echo and spin-echo EPI pulse sequence. In: Proceedings of the SMRM, 12th annual meeting, New York, p 169
166. Baker JR, Cohen MS, Stern CE, Kwong KK, Belliveau JW, Rosen BR (1992) The effect of slice thickness and echo time on the detection of signal changes during echo-planar functional neuroimaging. In: Proceedings of the SMRM, 11th annual meeting, Berlin, p 1822
167. Frahm J, Merboldt KD, Hanicke W, Kleinschmidt A, Steinmetz H (1993) High-resolution functional MRI of focal subcortical activity in the human brain. Long-echo time FLASH of the lateral geniculate nucleus during visual stimulation. In: Proceedings of the SMRM, 12th annual meeting, New York, p 57
168. Bruhn H, Kleinschmidt A, Boecker H, Merboldt K-D, Hanicke W, Frahm J (1994) The effect of acetazolamide on regional cerebral blood oxygenation at rest and under stimulation as assessed by MRI. *J Cereb Blood Flow Metab* 14:742-748
169. Ogawa S, Lee TM, Barrere B (1993) The sensitivity of magnetic resonance image signals of a rat brain to changes in the cerebral venous blood oxygenation. *Magn Reson Med* 29:205-210
170. deCrespigny AJ, Wendland MF, Derugin N, Kozniwska E, Moseley ME (1992) Real-time observation of transient focal ischemia and hyperemia in cat brain. *Magn Reson Med* 27:391-397
171. deCrespigny AJ, Wendland MF, Derugin N, Vexler ZS, Moseley ME (1993) Rapid MR imaging of a vascular challenge to focal ischemia in cat brain. *JMRI* 3:475-481
172. Bandettini PA, Aaron EA, Wong EC, Lowry TF, Hinks RS, Hyde JS, Forster HV (1994) Hypercapnia and hypoxia in the human brain: effects on resting and activation-induced MRI signal. In: Proceedings of the SMR, 2nd annual meeting, San Francisco, p 700
173. Prielmeier F, Nagatomo Y, Frahm J (1994) Cerebral blood oxygenation in rat brain during hypoxic hypoxia. Quantitative MRI of effective transverse relaxation rates. *Magn Reson Med* 31:678-681
174. Binder JR, Rao SM, Hammeke TA, Frost JA, Bandettini PA, Hyde JS (1994) Effects of stimulus rate on signal response during functional magnetic resonance imaging of auditory cortex. *Cogn Brain Res* 2:31-38
175. Rao SM, Bandettini PA, Bobholz J, Binder J, Hammeke TA, Frost JA, Hyde JS (1996) Relationship between movement rate and functional magnetic resonance signal change in primary motor cortex. *J Cereb Blood Flow Metab* 16:1250-1254
176. Sanders JA, Lewine JD, George JS, Caprihan A, Orrison WS (1993) Correlation of fMRI with MEG. In: Proceedings of the SMRM, 12th annual meeting, New York, p 1418
177. Connelly A, Jackson GD, Frackowiak RSJ, Belliveau JW, Vargha-Khadem F, Gadian DS (1993) Functional mapping of activated human primary cortex with a clinical MR imaging system. *Radiology* 188:125-130
178. Jack CR, Thompson RM, Butts RK, Sharbrough FW, Kelly PJ, Hanson DP, Riederer SJ, Ehman RL, Hangiandreou NJ, Cascino GD (1994) Sensory motor cortex: correlation of pre-surgical mapping with functional MR imaging and invasive cortical mapping. *Radiology* 190:85-92
179. Yablonsky DA, Haacke EM (1994) Theory of NMR signal formation in magnetically inhomogeneous tissue. Fast dephasing regime. *Magn Reson Med* 32:749-763
180. Wong EC, Bandettini PA (1993) A deterministic method for computer modelling of diffusion effects in MRI with application to BOLD contrast imaging. In: Proceedings of the SMRM, 12th annual meeting, New York, p 10
181. Boxerman JL, Hamberg LM, Rosen BR, Weisskoff RM (1995) MR contrast due to intravascular magnetic susceptibility perturbations. *Magn Reson Med* 34:555-566
182. Jesmanowicz A, Wong EC, Hyde JS (1993) Phase correction for EPI using internal reference lines. In: Proceedings of the SMRM, 12th annual meeting, New York, p 1239
183. Wong EC (1992) Shim insensitive phase correction for EPI using a two echo reference scan. In: Proceedings of the SMRM, 11th annual meeting, Berlin, p 4514
184. Prinster A, Pierpaoli C, Jezzard P, Turner R (1994) Simultaneous measurement of $\Delta R2$ and $\Delta R2^*$ in cat brain during hypoxia and hypercapnia. In: Proceedings of the SMR, 2nd annual meeting, San Francisco, p 439
185. Woods RP, Cherry SR, Mazziotta JC (1992) Rapid automated algorithm for aligning and reslicing PET images. *J Comput Assist Tomogr* 115:565-587

186. Friston KJ, Ashburner J, Frith CD, Poline J-B, Heather JD, Frackowiak R (1996) Spatial registration and normalization of images. *Human Brain Mapping* (in press)
187. Cohen JD, Noll DC, Schneider W (1993) Functional magnetic resonance imaging: overview and methods for psychological research. *Behav Res Methods Instr Comput* 25:101-113
188. LeBihan D, Jezzard P, Turner R, Cuenod CA, Pannier L, Prinster A (1993) Practical problems and limitations in using Z-maps for processing of brain function MR images. In: *Proceedings of the SMRM, 12th annual meeting, New York*, p 11
189. Sanders JA, Orrison WW (1993) ANOVA tests for identification of FMRI activation. In: *Proceedings of the SMRM, 12th annual meeting, New York*, p 1376
190. Schneider W, Casey BJ, Noll D (1994) Functional MRI mapping of stimulus rate effects across visual processing stages. *Human Brain Mapping* 1:117-133
191. Baker JR, Weisskoff RM, Stern CE, Kennedy DN, Jiand A, Kwong KK, Kolodny LB, Davis TL, Boxerman JL, Buchbinder BR, Wedeen VJ, Belliveau JW, Rosen BR (1994) Statistical assessment of functional MRI signal change. In: *Proceedings of the SMRM, 2nd annual meeting, San Francisco*, p 626
192. Biswal B, DeYoe EA, Cox RW, Hyde JS (1994) FMRI analysis for aperiodic task activation using nonparametric statistics. In: *Proceedings of the SMR, 2nd annual meeting, San Francisco*, p 624
193. Sychra JJ, Bandettini PA, Bhattacharya N, Lin Q (1994) Synthetic images by subspace transforms. I. Principal components images and related filters. *Med Phys* 21:193-201
194. Bandettini PA, Wong EC, DeYoe EA, Binder JR, Hinks RS, Hyde JS (1993) Fourier analysis of functional EPI time-course series. *JMRI* 3(P):89 (abstract)
195. Binder JR, Rao SM, Hammeke TA, Yetkin FZ, Jesmanowicz A, Bandettini PA, Wong EC, Estkowski LD, Goldstein MD, Haughton VM, Hyde JS (1994) Functional magnetic resonance imaging of human auditory cortex. *Ann Neurol* 35:662-672
196. Binder JR, Rao SM (1994) Human brain mapping with functional magnetic resonance imaging. In: Kertesz A (ed) *Localization and neuroimaging in neuropsychology*. Academic, San Diego, p 185
197. Binder JR, Rao SM, Hammeke TA, Frost JA, Cox RW, Wong EC, Bandettini PA, Jesmanowicz A, Hyde JS (1994) A lateralized, distributed network for semantic processing demonstrated with whole brain functional MRI. In: *Proceedings of the SMR, 2nd annual meeting, San Francisco*, p 694
198. Binder JR, Rao SM, Hammeke TA, Frost JA, Cox RW, Bandettini PA, Hyde JS (1994) Identification of auditory, linguistic, and attention systems with task subtraction functional MRI. In: *Proceedings of the SMR, 2nd annual meeting, San Francisco*, p 681
199. Singh M, Kim H, Kim T, Khosla D, Colletti P (1993) Functional MRI at 1.5 T during auditory stimulation. In: *Proceedings of the SMRM, 12th annual meeting, New York*, p 1431
200. Turner R, Jezzard P, LeBihan D, Prinster A, Pannier L, Zeffiro T (1993) BOLD contrast imaging of cortical regions used in processing auditory stimuli. In: *Proceedings of the SMRM, 12th annual meeting, New York*, p 1411
201. Rao SM, Bandettini PA, Wong EC, Yetkin FZ, Hammeke TA, Mueller WM, Goldman S, Morris GL, Antuono PG, Estkowski LD, Haughton VM, Hyde JS (1992) Gradient-echo EPI demonstrates bilateral superior temporal gyrus activation during passive word presentation. In: *Proceedings of the SMRM, 11th annual meeting, Berlin*, p 1827
202. Bates SR, Yetkin FZ, Bandettini PA, Jesmanowicz A, Estkowski L, Haughton VM (1993) Activation of the human cerebellum demonstrated by functional magnetic resonance imaging. In: *Proceedings of the SMRM, 12th annual meeting, New York*, p 1420
203. Cuenod CA, Zeffiro T, Pannier L, Posse S, Bonnerot V, Jezzard P, Turner R, Frank JA, LeBihan D (1993) Functional imaging of the human cerebellum during finger movement with a conventional 1.5 T MRI scanner. In: *Proceedings of the SMRM, 12th annual meeting, New York*, p 1421
204. Ellerman JM, Flament D, Kim S-G, Fu Q-G, Merkle H, Ebner TJ, Ugurbil K (1994) Spatial patterns of functional activation of the cerebellum investigated using high field (4 T) MRI. *NMR Biomed* 7:63-68
205. Kim S-G, Hendrich K, Hu X, Merkle H, Ugurbil K (1994) Potential pitfalls of functional MRI using conventional gradient-recalled echo techniques. *NMR Biomed* 7:69-74
206. Kim S-G, Ashe J, Georgopoulos AP, Merkle H, Ellermann JM, Menon RS, Ogawa S, Ugurbil K (1993) Functional imaging of human motor cortex at high magnetic field. *J Neurophysiol* 69:297-302

207. Rao SM, Binder JR, Hammeke TA, Lisk LM, Bandettini PA, Yetkin FZ, Morris GL, Mueller WM, Antuono PG, Wong EC, Haughton VM, Hyde JS (1993) Somatotopic mapping of the primary motor cortex with functional magnetic resonance imaging. In: Proceedings of the SMRM, 12th annual meeting, New York, p 1397
208. Rao SM, Binder JR, Hammeke TA, Bandettini PA, Bobholz J, Frost JA, Myklebust BM, Jacobson RD, Hyde JS (1995) Somatotopic mapping of the human primary motor cortex with functional magnetic resonance imaging. *Neurology* 45:919-924
209. DeYoe EA, Carman GJ, Bandettini PA, Glickman S, Weiser J, Cox R, Miller D, Neitz J, Mapping Striate and extrastriate areas in human cerebral Cortex. *PNAS* (1996) 93:2382-2386
210. DeYoe EA, Neitz J, Miller D, Wieser J (1993) Functional magnetic resonance imaging (fMRI) of visual cortex in human subjects using a unique video graphics stimulator. In: Proceedings of the SMRM, 12th annual meeting, New York, p 1394
211. Bandettini PA, Rao SM, Binder JR, Hammeke TA, Jesmanowicz A, Yetkin FZ, Bates S, Estkowski LD, Wong EC, Haughton VM, Hinks RS, Hyde JS (1993) Magnetic resonance functional neuroimaging of the entire brain during performance and mental rehearsal of complex finger movement tasks. In: Proceedings of the SMRM, 12th annual meeting, New York, p 1396
212. DeLaPaz RL, Hirsch J, Relkin N, Victor J, Bartoshuk L, Norgren R, Prichard T (1994) Human gustatory cortex localization with functional MRI. In: Proceedings of the SMR, 2nd annual meeting, San Francisco, p 335
213. Kim S-G, Ashe J, Hendrich K, Ellerman JM, Merkle H, Ugurbil K, Georgopoulos AP (1993) Functional magnetic resonance imaging of motor cortex: hemispheric asymmetry and handedness. *Science* 261:615-616
214. Jezzard P, Karni A, Meyer G, Adams M, Prinster A, Ungerleider L, Turner R (1994) Practice makes perfect: a functional MRI study of long term motor cortex plasticity. In: Proceedings of the SMR, 2nd annual meeting, San Francisco, p 330
215. Ellerman JM, Flament D, Kim S-G, Merkle H, Andersen P, Ebner T, Ugurbil K (1994) Cerebellar activation due to error detection/correction in a visuo-motor learning task: a functional magnetic resonance imaging study. In: Proceedings of the SMR, 2nd annual meeting, San Francisco, p 331
216. Rao SM, Binder JR, Hammeke TA, Harrington DL, Haaland KY, Bobholz JA, Frost JA, Myklebust BM, Jacobson RD, Bandettini PA, Hyde JS (1994) Functional magnetic resonance imaging correlates of cognitive motor learning: preliminary findings. In: Proceedings of the SMR, 2nd annual meeting, San Francisco, p 329
217. McCarthy G, Blamire AM, Rothman DL, Gruetter R, Shulman RG (1993) Echo-planar magnetic resonance imaging studies of frontal cortex activation during word generation in humans. *Proc Natl Acad Sci USA* 90:4952-4956
218. Hinke RM, Hu X, Stillman AE, Kim S-G, Merkle H, Salmi R, Ugurbil K (1993) Functional magnetic resonance imaging of Broca's area during internal speech. *Neuroreport* 4:675-678
219. Rueckert L, Appollonio I, Grafman J, Jezzard P, Johnson R, Jr, LeBihan D, Turner R (1994) Magnetic resonance imaging functional activation of left frontal cortex during covert word production. *J Neuroimaging* 4:67-70
220. Menon R, Ogawa S, Tank DW, Ellermann JM, Merkle H (1993) Visual mental imagery by functional brain MRI. In: Proceedings of the SMRM, 12th annual meeting, New York, p 1381
221. Ogawa S, Tank DW, Menon R, Ellermann JM, Merkle H, Ugurbil K (1993) Functional brain MRI of cortical areas activated by visual mental imagery. In: Book of abstracts, Society for Neuroscience, 23rd annual meeting, Washington DC, p 976
222. Rao SM, Binder JR, Bandettini PA, Hammeke TA, Yetkin FZ, Jesmanowicz A, Lisk LM, Morris GL, Mueller WM, Estkowski LD, Wong EC, Haughton VM, Hyde JS (1993) Functional magnetic resonance imaging of complex human movements. *Neurology* 43:2311-2318
223. Tyszka JM, Grafton ST, Chew W, Woods RP, Colletti PM (1994) Parceling of mesial frontal motor areas during movement using functional magnetic resonance imaging at 1.5 tesla. *Ann Neurol* 35:746-749
224. Binder JR, Rao SM, Hammeke TA, Yetkin FZ, Wong EC, Mueller WM, Morris GL, Hyde JS (1993) Functional magnetic resonance imaging (fMRI) of auditory semantic processing. *Neurology* 43 [Suppl 2]:189 (abstract)
225. Binder JR, Rao SM, Hammeke TA, Frost JA, Bandettini PA, Jesmanowicz A, Hyde JS (1995) Lateralized human brain language systems demonstrated by task subtraction functional magnetic resonance imaging. *Arch Neurol* 52:593-601
226. Cohen JD, Perlstein WM, Braver TS, Nystrom LE, Noll DC, Jonides J, Smith EE, (1997) *Nature* 386 (6625):604-608

227. Cohen JD, Forman SD, Casey BJ, Noll DC (1993) Spiral-scan imaging of dorsolateral prefrontal cortex during a working memory task. In: Proceedings of the SMRM, 12th annual meeting, New York, p 1405
228. Blamire AM, McCarthy G, Nobre AC, Puce A, Hyder F, Bloch G, Phelps E, Rothman DL, Goldman-Rakic P, Shulman RG (1993) Functional magnetic resonance imaging of human pre-frontal cortex during a spatial memory task. In: Proceedings of the SMRM, 12th annual meeting, New York, p 1413
229. LeBihan D, Turner R, Zeffiro T, Cuenod CA, Jezzard P, Bonnerot V (1993) Activation of human primary visual cortex during visual recall: a magnetic resonance imaging study. *Proc Natl Acad Sci USA* 90:11802-11805
230. Tootell RBH, Kwong KK, Belliveau JW, Baker JR, Stern CE, Savoy RL, Breiter H, Born R, Benson R, Brady TJ, Rosen BR (1993) Functional MRI (fMRI) evidence for MT/V5 and associated visual cortical areas in man. In: Book of abstracts, Society for Neuroscience, 23rd annual meeting, Washington DC, p 1500
231. Karni A, Ungerleider L, Haxby J, Jezzard P, Cuenod CA, Turner R, LeBihan D (1993) Stimulus dependent MRI signals evoked by oriented line-element textures in human visual cortex. In: Book of abstracts, Society for Neuroscience 23rd annual meeting, Washington DC, p 1501
232. Sorensen AG, Caramia F, Wray SH, Kwong K, Belliveau J, Stern C, Baker J, Gazit I, Breiter H, Rosen B (1993) Extrastriate activation in patients with visual field defects. In: Proceedings of the SMRM, 12th annual meeting, New York, p 62
233. Tootell RBH, Reppas JB, Dale AD, Look RB, Malach R, Brady TJ, Rosen BR (1996) Visual motion aftereffect in human cortical area MT/V5 revealed by functional magnetic resonance imaging. *Nature* 375:139-141
234. Sereno MI, Dale AM, Kwong KK, Belliveau JW, Brady TJ, Rosen BR, Tootell RBH (1995) Functional MRI reveals borders of multiple visual areas in humans. *Science* 268:889-893
235. Hedera P, Lai S, Haacke EM, Lerner AJ, Hopkins AL, Lewin JS, Friedland RP (1994) Abnormal connectivity of the visual pathways in human albinos demonstrated by susceptibility-sensitized MRI. *Neurology* 44:1921-1926
236. Cao Y, Vikingstad EM, Huttenlocher PR, Towle VL, Levin DN (1994) Functional magnetic resonance studies of the reorganization of the human hand sensorimotor area after unilateral brain injury in the perinatal period. *Proc Natl Acad Sci USA* 91:9612-9616
237. Renshaw PF, Yurgelun-Todd DA, Cohen BM (1994) Greater hemodynamic response to photic stimulation in schizophrenic patients: an echo planar MRI study. *Am J Psychiatry* 151:1493-1495
238. Jackson GD, Connelley A, Cross JH, Gordon I, Gadian DG (1994) Functional magnetic resonance imaging of focal seizures. *Neurology* 44:850-856
239. Wenz F, Schad LR, Baudendistel K, Flomer F, Schroder J, Knopp MV (1993) Effects of neuroleptic drugs on signal intensity during motor cortex stimulation: functional MR-imaging performed with a standard 1.5 T clinical scanner. In: Proceedings of the SMRM, 12th annual meeting, New York, p 1419
240. Breiter HC, Kwong KK, Baker JR, Stern CE, Belliveau JW, Davis TL, Baer L, O'Sullivan RM, Rauch SL, Savage CR, Cohen MS, Weisskoff RM, Brady TJ, Jenike MA, Rosen BR (1993) Functional magnetic resonance imaging of symptom provocation in obsessive-compulsive disorder. In: Proceedings of the SMRM, 12th annual meeting, New York, p 58
241. Breiter HC, Rauch SL, Kwong KK, Baker JR, Weisskoff RM, Kennedy DN, Kendrick AD, Davis TL, Jiang A, Cohen MS, Stern CE, Belliveau JW, Baer L, O'Sullivan RL, Savage CR, Jenike MA, Rosen BR (1996) Functional magnetic resonance imaging of symptom provocation in obsessive compulsive disorder. *Arch Gen Psychiatry* 53:595-605
242. Cao Y, Towle VL, Levin DN, Grzeszczuk R, Mullian JF (1993) Conventional 1.5 T functional MRI localization of human hand sensorimotor cortex with intraoperative electrophysiologic validation. In: Proceedings of the SMRM, 12th annual meeting, New York, p 1417
243. Morris GL, Mueller WM, Yetkin FZ, Haughton VM, Hammeke TA, Swanson S, Rao SM, Jesmanowicz A, Estkowski LD, Bandettini PA, Wong EC, Hyde JS (1994) Functional magnetic resonance imaging in partial epilepsy. *Epilepsia* 35:1194-1198
244. Turner R, Jezzard P (1994) Magnetic resonance studies of brain functional activation using echo-planar imaging. In: Thatcher RW, Hallett M, Zeffiro T, John ER, Huerta M (eds) Functional neuroimaging. Technical foundations. Academic, San Diego, pp 69-78
245. Schulman RG, Blamire AM, Rothman DL, McCarthy G (1993) Nuclear magnetic resonance imaging and spectroscopy of human brain function. *Proc Natl Acad Sci USA* 90:3127-3133
246. Prichard JW, Rosen BR (1994) Functional study of the brain by NMR. *J Cereb Blood Flow Metab* 14:365-372

247. Cohen ME, Bookheimer SY (1994) Localization of brain function using magnetic resonance imaging. *Trends Neurosci* 17:1994
248. Bandettini PA, Binder JR, DeYoe EA, Hyde JS (1996) Sensory activation-induced hemodynamic changes observed in the human brain with echo planar MRI. In: Grant DM, Harris RK (eds) *Encyclopedia of nuclear magnetic resonance imaging*. Wiley & Sons Ltd, Chichester (1996) pp 1051-1056